Compressibility of the polymer crystal

Taisuke Ito
Faculty of Polytechnic Sciences, Kyoto Institute of Technology, Matsugasaki, Kyoto 606, Japan
(*Received* 6 *December* 1980)

Results for the compressibilities of a wide range of polymer crystals along the fibre- and the transverse crystal axes are presented. Good agreement is found between the theoretical and the experimental results of different authors.

Keywords Compressibility; polymer crystal; high pressure; X-ray diffraction; equation of state; polyethylene; hydrogen bond

INTRODUCTION

It has long been recognized that bulk crystalline polymers consist of heterogeneous regions. Essentially, there are two of these: crystallite and amorphous or non-crystalline. Crystallite size, estimated by X-ray diffraction or by electron microscopy, ranges in general from 10^2 to 10^3 Å. Thus, the mechanical properties exhibited by bulk crystalline polymers always result from the simultaneous and often unresolvable contributions from these heterogeneous regions.

Several theoretical treatments[1-5] have been published attempting to predict mechanical performance on the basis of a limited number of factors such as the elastic constants of both crystallite and the non-crystalline region, methods of coupling the two regions, crystallinity, chain orientation, etc. Achievement of much enhanced mechanical properties by the ultra-high orientation processing[6-8] has shown these treatments to be of increasing practical importance in estimating limiting mechanical properties. Thus elastic constants are of basic importance.

The crystal is defined as the most compact, regular aggregate of molecules which gives the upper limiting elastic constants possible. Sakurada and coworkers[9-11] studied the Young's moduli of the crystal of polymer (after work by Dulmage and Contois[12]), applying X-ray diffraction to a highly-oriented bulk specimen. From a study of the increase in lattice spacing, the mean value of the strain in the plane normal to the direction of the crystallites held under uniaxial tension was obtained. However, it was experimentally much more difficult to measure the *stress* exerted in the crystallites. They therefore assumed that the stress was homogeneous within the specimen (corresponding to the Reuss model[13]) and put the bulk stress equal to the stress in the crystallites. Geil *et al.*[14] recently tackled the stress–strain curve for a piece of a single crystal of orthorhombic polyethylene, employing a microtechnique, but apart from this the Sakurada approach is still the only way to obtain stress–strain relationships for polymer crystals.

However, there is another type of stress which is relevant, i.e. hydrostatic pressure. Hydrostatic pressure is a more advantageous property than uniaxial stress for the following reasons.

First, no calibration due to deformation of the bulk specimen is needed to obtain the true stress. For an anisotropic homogeneous body of material which is submerged in liquid under pressure P, an arbitrary plane experiences only pure hydrostatic pressure, normal to that plane and equal to the pressure P; there are no components of shearing stress.

Second, there is no restriction, in principle, upon the upper limit the hydrostatic stress can take. For uniaxial stress, the upper limit is determined by the strength of the bulk specimen and is often too low to give a lattice strain observable with sound accuracy. Third, it was found that strains induced by the hydrostatic pressure in the polymer crystallites are completely recoverable[15] upon removal of the load: creep, which is inherent in bulk polymeric materials subjected to uniaxial stress, does not take place to any appreciable extent[15]. All of the above factors favour clearer experimental results.

Finally, hydrostatic compression yields an equation of state for the polymer, only recently discovered.

To apply a hydrostatic pressure, however, homogeneous stress must be assumed if we are to find the pressure acting on the crystallites. If this holds for uniaxial stress, the microstructure model consisting of crystalline and non-crystalline regions connected in series must hold for the oriented bulk specimen, both in the longitudinal (parallel)[12] and the transverse (perpendicular)[16] directions to the fibre axis of the drawn specimen. For hydrostatic compression, the homogeneous stress assumption is affected to a much smaller degree by bulk specimen microstructure since this holds as long as the non-crystalline region transmits the pressure as a liquid medium. This is most likely when time is allowed for pressure equilibration. Experimental evidence for this will be given below.

Theoretically[17-28], a considerable body of theory has been developed, particularly for polyethylene. To a first approximation, the contraction of the molecular crystal by hydrostatic compression corresponds to the decrease in the distance between the non-bonded atoms of the adjacent chains. The free energy increase due to such a contraction of the molecular crystal will be estimated[27,29] if the coordinates of the non-bonded atoms concerned are known together with their potential energy function and the volume dependence of the frequencies of the associated vibrations. Without the last parameter, the 0K

0032/3861/82/101412-23$03.00

compressibility and the pressure–volume (P–V) relationships can be calculated. Müller[17], pioneering the X-ray diffraction technique under high hydrostatic pressures, used a beryllium (Be) metal cell to calculate the 0K compressibilities of paraffin crystals and compared them with his own experimental results. Since then, calculation of the compressibility and the equation of state of the paraffinic crystals has been refined by several authors.

Several articles have been published on the effects of the hydrostatic pressure on the compressibility of bulk material of polymers[30]. This review concerns the crystal lattice of polymers, not the bulk material. The specimen used in the experiments described is, however, a bulk crystalline polymer, 0.1–1 mm (excepting the case reported by Miyaji[31] who used a mat sample of polyoxymethylene single crystal). The term 'polymer crystal' is used for convenience, instead of 'polymer crystallite' or 'polymer crystalline region' which are strictly correct. An *a priori* assumption will further be made that there is no difference in compressible properties between the crystallite and a single crystal of infinite size.

THEORY

The Helmholtz free energy A of a crystal is given[21,27,32] by the sum of the lattice energy U and the normal modes or phonon vibration energy A_{vib}, as expressed[27] by equation (1):

$$A = U + A_{vib} \tag{1}$$

U may be calculated from the coordinates of the non-bonded atoms in the crystal and the interatomic potential functions associated with them, as

$$U = \tfrac{1}{2}\sum_{ij} V_{ij}(r_{ij}), \tag{2}$$

where the potential is denoted by V_{ij} as function of the distance r_{ij} between the ith and jth atoms. Because the interatomic potential function is generally treated as independent of temperature, U is determined solely by the distances between non-bonded atoms. It may be described as a function of volume as long as the unit cell dimensions and the coordinates of the atoms within it are known.

A_{vib} is given by equation (3) for a crystal which is treated as a set of harmonic oscillators:

$$A_{vib} = \sum_j \tfrac{1}{2}h\nu_j + \sum_j kT \ln[1 - \exp(-h\nu_j/kT)] \tag{3}$$

where ν_j is the normal frequency of the jth mode, k the Boltzmann constant, h Planck's constant and T the absolute temperature. The first term on the right-hand side of equation (3),

$$\sum_j \tfrac{1}{2}h\nu_j \tag{4}$$

is the zero point energy (ZE). The second term may be calculated according to[27]:

$$\sum_j kT \ln[1 - \exp(-h\nu_j/kT)] = N^{-1}kT\sum_{k,i} \ln[2\sinh(h\nu_i(\mathbf{k})/2kT)], \tag{5}$$

where $\nu_i(\mathbf{k})$ denotes the normal frequency of the ith branch at the point $\mathbf{k}$ in the reciprocal space and N the number of points taken in the computation. Since the potential energy function V_{ij} is anharmonic, the normal mode frequency calculated using the force constant derived from V_{ij} varies with volume. For this reason, the calculation based on equation (3) on the one hand and the anharmonic V_{ij} on the other is equivalent to an approximation using a 'quasiharmonic' oscillator.

Differentiating the Helmholtz free energy with respect to volume, we find the pressure P of the crystal,

$$P = -(\partial A/\partial V)_T \tag{6}$$

Substituting equation (3) into equation (1) and differentiating, P is:

$$P = -\frac{dU}{dV} + \frac{1}{V}\sum_j \tfrac{1}{2}\gamma_j h\nu_j + \frac{1}{V}\sum_j \gamma_j \frac{h\nu}{\exp(h\nu_j/kT) - 1} \tag{7}$$

In equation (7), $\gamma_j = -(V/\nu_j)(d\nu_j/dV)$ is called the Grüneisen parameter for the jth oscillator and reflects the anharmonicity of the force field. It is positive because ν_j increases[33] with decreasing volume.

Pressure P is divided into three parts as follows:

$$P = P_L P_{ZE} + P_T \tag{8}$$

where:

$$P_L = -\frac{dU}{dV} \tag{9}$$

$$P_{ZE} = \frac{1}{V}\sum_j \tfrac{1}{2}\gamma_j h\nu_j \tag{10}$$

and

$$P_T = \frac{1}{V}\sum_j \gamma_j \frac{h\nu_j}{\exp(h\nu_j/kT) - 1} \tag{11}$$

In equation (8), P_L is the pressure contributed by a 'spring' of lattice and can take positive or negative values according to whether the volume of the crystal is smaller or larger than that at absolute zero. P_{ZE} and P_T are the zero point vibration and the thermal vibration of the harmonic oscillator. Kobayashi[27] applied the perturbation theory of Kitagawa and Miyazawa[34] to the calculation of P_{ZE} and P_T. Here it is worth while noting that thermal vibration energies of the harmonic oscillator, by themselves, never contribute to the pressure. It is only because γ_js are different from zero that they contribute to the pressure.

Equation (7) now provides the theoretical basis for obtaining the equation of state of a crystal composed of 'quasiharmonic' oscillators.

MATERIALS AND SAMPLE PREPARATION

Polymers studied by various authors are
high density polyethylene (HDPE)[15,37,38,44–51];
low density polyethylene (LDPE)[41,45,46];
polytetrafluoroethylene form II (PTFE(II)) at 10°[50,52] and form IV (PTFE(IV)) at 24°C[50,52];
isotactic polypropylene (it-PP)[46,50,53];
isotactic poly(1-butene) (it-P1B)[41,50];

Table 1 Drawing and annealing conditions for the X-ray sample*

Polymer	Material: Grade	Material: Manufacturer	Moulding temp. (°C)	Drawing: Temp. (°C)	Drawing: Draw ratio	Annealing: Temp. (°C)	Annealing: Time (min)	Annealing: Tension	Density at 30°C (g cm^{-3})	Notes
it-PP	HFO-J400	Mitsui Petrochemical Industries	200	120	6.0	120	60	C	0.905	
it-P1B	Experimental	Exxon	150	100	9.0	110	60	C	0.910	
it-P4M1P	TPX-RT20	ICI Japan	278	170	6.5	200	30	C	0.831	
PTFE	Polyflon M-12	Daikin Kogyo	–	235	3.2	235	60	C	2.088	
PVDF(I)	KF (sheet)	Kureha Chemical Industries	–	room temp.	4.5	268	60(W)	C	1.775	Annealed at 4.0 kbar (T)
PVDF(I)	KF (chip)	*Ibid*	200	75	4.2	120	30(w)	C	1.775	
PVDF(II)	KF (chip)	*Ibid*	210	160	5.0	150	600	F	1.788	
POM	Delrin 100x	DuPont	190	160	6.0(rd)	160	5	C	1.422	
PEO	PEO-18	Seitetsu Kagaku	100	60	5.0	60	60	C	1.215	
PTMO	Experimental	Our laboratory	55	40	5.0(rd)	30	90	C	–	
PET	Unitika-Ester	Unitika	270	73	4.0	210	20	L	1.342	
PEOB(α)	Experimental	Unitika	250	76	3.3	200	60	F	1.337	
Ny-6(α)	1030B	Ube Industries	250	150	4.0	135	1440(w)	C	1.145	
Ny-6(γ)	1030B	*Ibid*	–	150	3.0	195	20	L	1.142	
at-PVA	PVA-E	Kuraray	cast(w)	150	4.0	225	5	C	1.305	
at-PVA	Experimental (bristle)	–	–	80	6.0(dr)	225	5	C	1.302	

* For polyethylenes, see *Table 3*. W, in Wood's metal; w, in water; C, at constant length in an air heating-bath (unless noted); F, under free length in a small cylinder dipped in a silicone oil heating-bath; L, under free length, lapped with aluminium foil and dipped in silicone oil heating-bath; rd, initially roll-drawn and then uniaxially drawn; dr, uniaxially drawn and then rolled; (T), this sample which gave sharp equatorial reflections was supplied by Professor Takemura of Kyushu University

isotactic poly(4-methyl-1-pentene) (it-P4M1P)[46,50,54];
polyoxymethylene (POM)[31,41,46,49,50];
poly(ethylene oxide) form I (PEO(I))[41,55];
poly(tetramethylene oxide) form I (PTMO(I))[41,50];
poly(ethylene *p*-oxybenzoate) α-form (PEOB(α)[41,50,56];
nylon-6 α-form and γ-form (Ny-6(α) and Ny-(6(γ))[50,57,58];
atactic poly(vinyl alcohol) (at-PVA)[58,59];
poly(vinylidene fluoride) form I and form II (PVDF(I) and PVDF(II))[41,60];
carbon fibre derived from polyacrylonitrile fibre[41,50,51,61].

Here, the orthorhombic crystal of HDPE is abbreviated as *o*-PE.

Ito and coworkers used compressibility samples prepared as follows. Solid chips, with the exception of at-PVA and carbon fibre, were melt-pressed between the two metal plates of a hot hydraulic press. A plate of thickness 2–3 mm was obtained which, when hot-drawn to a draw ratio of several times, gave a sheet with a thickness suitable for preparing rod samples for X-ray diffraction. Each drawn sheet was given ample annealing treatment in an air bath or by lapping the sample with aluminium foil, in a silicone oil bath. This is essential to obtain stable crystal structures and sharp X-ray reflections. Detailed procedures for preparing Ny-6(α), Ny-6(γ) and at-PVA are described in ref 58. The annealing conditions, draw ratio and the density of the drawn and annealed samples at 30°C are summarized in *Table 1*.

A highly graphitized carbon fibre was supplied by Toray Industires, Inc. It was made from polyacrylonitrile fibre and had a density of 2.083 g cm^{-3} at 30°C. Natural graphite (supplied by Nippon Cargon Co., grade SAD, ash content less than 0.01%) was used as the reference material for the carbon fibre and had a density of 2.126 g cm^{-3} at 30°C. The 002 spacings of these samples were, respectively, 3.384 and 3.362 Å, compared with the reported value[62] of 3.354 Å.

An unoriented, well-crystallized HDPE sample was prepared from Sholex 6050 (Showa Denko Co.), and was moulded at 165°C in a hot press, followed by cooling in the press to 120°C, annealing at this temperature for 3 h and cooling to room temperature by shutting off the press-heaters. This unoriented specimen had a density of 0.968 g cm^{-3} at 30°C.

Low molecular weight organic crystalline substances were used as reference materials. These were n-heptacosane[45,46,49–51] adamantane[41,49,50], hexamethylenetetramine[41,50], pentaerythritol[41,50], which were purified by recrystallization and had melting points of, respectively, 59.6°–61.2°, 269.0°–270.5°, >259° (sub.) and 249.2°–251.5°C. The low molecular weight crystals were ground in an agate mortar to give a fine continuous powder diagram. The powder sample was packed directly in the hole of a Be-cell[15]. Mixing a silicone grease with the powder sample, to soften the specimen and transmit the hydrostatic pressure in a more even manner, gave the same resultsas t/ose for pure powder crystals.

A powder sample of natural daamgnd was supplied by Sanwa Diaeond Industries, Inc. Average particle size was 0.5 μm diameter.

RESULTS AND DISCUSSION[41,49–51]

POLYETHYLENE

Results

The diffraction lines obtained from the equatorial planes and the basal (002) plane of *o*-PE at 20°C at increasing pressures up to 8 kbar are shown in *Figures 1a* and *1b*, respectively.

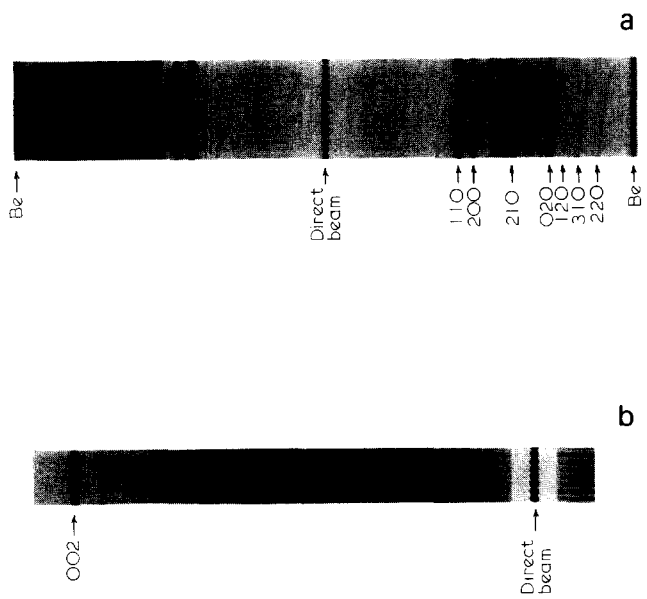

Figure 1 X-ray diffraction patterns for (a) the equatorial and (b) the basal 002 reflections of drawn and annealed HDPE. Pressures (kg cm^{-2}) (from the bottom): (a) 1 (normal pressure), 500, 1000, 1500, 2000, 2500, 3000, 4000, 5000, 6000, 7000, 8000, 1 (normal pressure) and 167 (residual pressure); (b) 1, 1000, 2000, 3000, 4000, 5000, 1 and 76. Pressure medium: water

The indices of the lines in *Figure 1a* are (starting at low angles) 110, 200, 210, 020, 120, 310 and 220, respectively. Exposure time was 20 min for the intense 110 and 200 reflections and 90 min for the others. This was achieved by blocking out the former reflections with a brass shield.

The equatorial diffractions in *Figure 1a* shift towards higher angles with increasing pressure, i.e. the interplanar spacings decrease with increasing pressure. Meanwhile the 002 reflections in *Figure 1b* remain at almost the same angle. In both cases, visual inspection indicates that the widths and the intensities of the diffraction maxima are approximately constant under the range of high pressures.

Some residual pressure remains because of the friction of the Bridgman seal when the pressure is released (after each experiment the high pressure gauge was checked to ensure that the zero point had been recovered). The residual pressure causes a residual shift of the diffraction lines from the positions registered before the pressure was applied (see the exposed zones at the bottom and second from the top in *Figure 1a*).

Such slight residual shifts do not result from non-elastic strain of the crystal lattice. This phenomenon, found in *o*-PE crystal (the hydrostatic pressure (8 kbar) has little effect on leaving any unrecovered, non-elastic strain) is commonly found in the other polymer crystals. Also, the responses of the strains were found to be elastic within the time scale of the X-ray exposures, as in *Figure 2* where the pressure was raised to 3000 kg cm^{-2} over a period of 60 s and kept constant for about 6 h. In *Figure 2*, the strain in the (110) plane, $\varepsilon_{(110)}$, is defined by equation (12), which gives the linear strain of the crystal normal to the observed lattice plane:

$$\varepsilon_{(hkl)} = \frac{\Delta d}{d_{0,(hkl)}} \qquad (12)$$

where $d_{0,(hkl)}$ is the spacing of (hkl) plane at normal pressure and Δd is the increment induced by applying a high pressure. The strain behaviour of the (110) plane is elastic under pressurizing–releasing pressure cycles, giving a constant $\varepsilon_{(110)}$ under constant pressure& The same concdusion was obtained wit/ the 200! plane.

Figure 3 shows strain $\varepsilon_{(hkl)}$ vs. pressure relationships for *o*-PE (200), (020), (110), (011) and (002) planes. The curves seen in *Figure 3* show the strain per unit stress decreasing with increasing stress; this originates from the anharmonicity of the potentials which work in the force field among the constituent non-bonded atoms. The equatorial $(hk0)$ planes give rise to transverse strains perpendicular to the fibre-axis, while the basal (002) plane generates a longitudinal strain parallel to the fibre-axis and along the chain. In *Figure 3*, $-\varepsilon_{(hk0)}$ values amount to 4.0–4.5% at 7.85 kbar, with the strain in the *a*-axis direction $\varepsilon_{(200)}$ always being greater than that in the *b*-axis direction $\varepsilon_{(020)}$. In the fibre-axis direction, the *o*-PE crystal is essentially incompressible ($-\varepsilon_{(002)}=0.066\%$ at 5 kbar) and can even be compared with the incompressible behaviour of the (111) plane of diamond[50].

The spacing of each lattice plane at normal pressures was confirmed to fit to an orthorhombic unit cell[63]. Further, it was found that under applied pressures, the spacing and the strain of each lattice plane satisfied

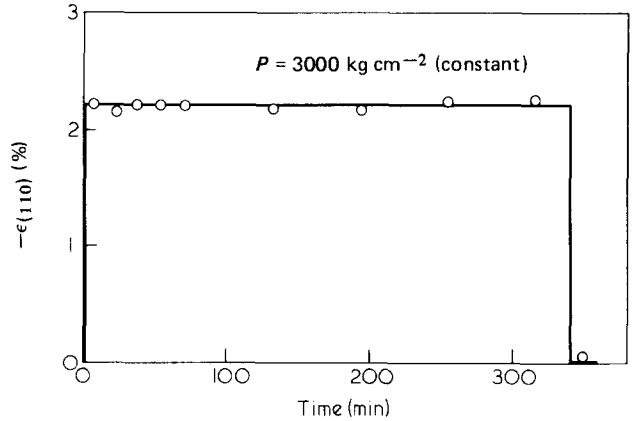

Figure 2 Strain in the (110) plane for drawn and annealed HDPE plotted against time under a constant pressure of 3000 kg cm^{-2}

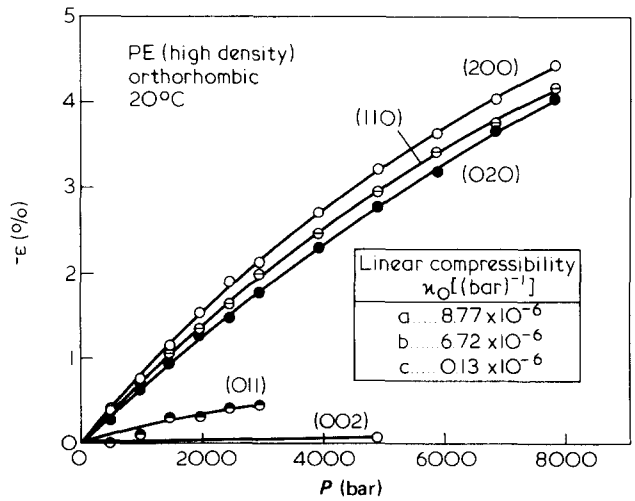

Figure 3 Pressure–strain curves for *o*-PE crystal at 20°C. Full line indicates the third order polynomial fitted by least squares

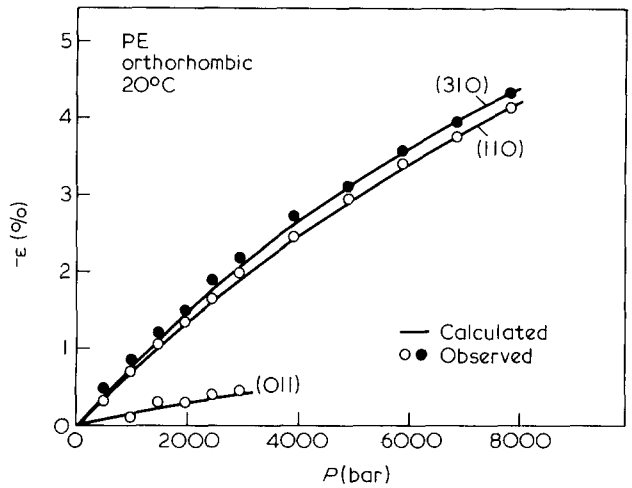

Figure 4 Comparison between calculated (full line) and observed strains for the 110, 310 and 011 *o*-PE reflections, showing the conservation of the orthorhombic structure under the high pressures

(within the experimental error) the following orthorhombic relationships:

$$1/d^2_{(hkl)} = h^2/a^2 + k^2/b^2 + l^2/c^2 \quad (13)$$

and

$$\varepsilon_{(hkl)}/d^2_{0,(hkl)} = h^2\varepsilon_a/a_0^2 + k^2\varepsilon_b/b_0^2 + l^2\varepsilon_c/c_0^2 \quad (14)$$

where $d_{(hkl)}$, a, b and c are the spacing of (hkl) plane and the three lattice constants of the orthorhombic cell under applied pressure; a_0, b_0 and c_0 are the lattice constants at normal pressures; and ε_a, ε_b and ε_c are the linear strains along the a-, b- and c-axes. This is shown in *Figure 4* where the strains in the (110), (310) and (011) planes, calculated using equation (14) from the observed $\varepsilon_{(200)}$, $\varepsilon_{(020)}$ and $\varepsilon_{(002)}$, are seen to be in good agreement with observed values. The conclusion is therefore that the *o*-PE crystal deforms under pressure at room temperature while retaining its orthorhombic structure. No phase transition occurs up to 8 kbar. This evidence has been extended by Hikosaka, Minomura and Seto[38] to a pressure of 45 kbar. Thus the volumetric strain can easily be obtained by calculation from the observed linear strains along the principal axes. These and the calculated volumetric strains can be represented by third order polynomials as functions of pressure. By least squares fitting, these are as follows, where pressure is measured in bars:

$$-\varepsilon_{(200)} = 8.77\times10^{-6}P - 0.54\times10^{-9}P^2 + 0.018\times10^{-12}P^3 \quad (15)$$

$$-\varepsilon_{(020)} = 6{,}72\times10^{-6}P - 0.24\times10^{-9}P^2 + 0.005\times10^{-12}P^3 \quad (16)$$

$$-\varepsilon_{(002)} = 0.13\times10^{-6}P \quad (17)$$

$$-\Delta V/V_0 = 15.6\times10^{-6}P - 0.84\times10^{-9}P^2 + 0.030\times10^{-12}P^3 \quad (18)$$

In equation (18), ΔV is defined by $\Delta V = V_P - V_0$ where V_P and V_0 are the volumes of the crystal at pressure P and at normal pressure, respectively. At 293K, V_0 for *o*-PE is 0.9994 $cm^3\ g^{-1}$.[64] It should be emphasized that these equations are applicable only at pressures below 7850 bar (8000 kg cm^{-2}).

It is clear from *Figure 3* and from equations (15)–(17) that the linear strains in directions perpendicular to the fibre-axis in *o*-PE are larger by two orders of magnitude than those parallel to the fibre-axis. Such anisotropy of the linear strains between the fibre-axial and the lateral directions is inherent to the polymer crystal, whose structure consists of covalently bound chains held loosely in bundles by the weak secondary forces. In *o*-PE crystal, the chain is in the fully-extended planar zigzag conformation and has a large Young's modulus[9–11], comparable with that of diamond; the lateral cohesion forces, however, are typical of non-polar van der Waals forces in paraffinic crystals. The linear strains as well as the initial linear compressibility κ_0, defined as:

$$\kappa_{0,(hkl)} = \frac{1}{d_{0,(hkl)}}\left(\frac{\partial d_{(hkl)}}{\partial P}\right)_{T;P\to0} = \left(\frac{\partial \varepsilon_{(hkl)}}{\partial P}\right)_{T;P\to0} \quad (19)$$

are found to be smaller in the b-axis direction than along the a-axis. This anisotropy in linear compressibility is consistent with the anisotropy in the Young's moduli demonstrated by Sakurada *et al.*[15], who obtained $E_{(200)} = 3.1\times10^4$ bar and $E_{(020)} = 3.8\times10^4$ bar, where E is the Young's modulus. Here, the inversion in magnitude of the relation between stiffness and compliance was taken into account. Essentially the same results as described above on *o*-PE crystal were obtained by several other authors; these will appear later in the text.

We recall at this stage that our conclusions, equations (15)–(18), are based on the assumption that the non-crystalline part of the specimen transmits the hydrostatic pressure as a liquid medium. Experimental support for this assumption is desirable. This is given in *Figure 5*

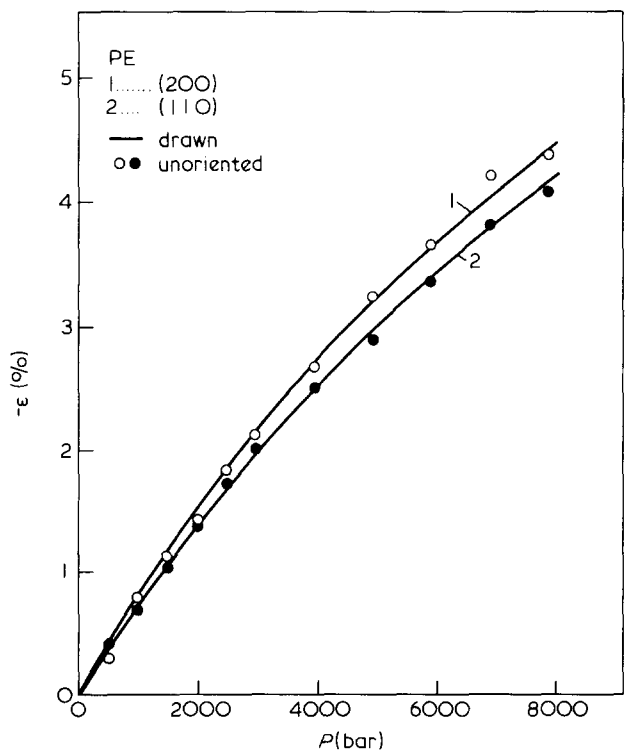

Figure 5 Comparison of the strains in the (200) and (110) planes between the drawn (full line) and the unoriented (open and full circles) specimens, giving support for the assumption of the homogeneous pressure transmittance

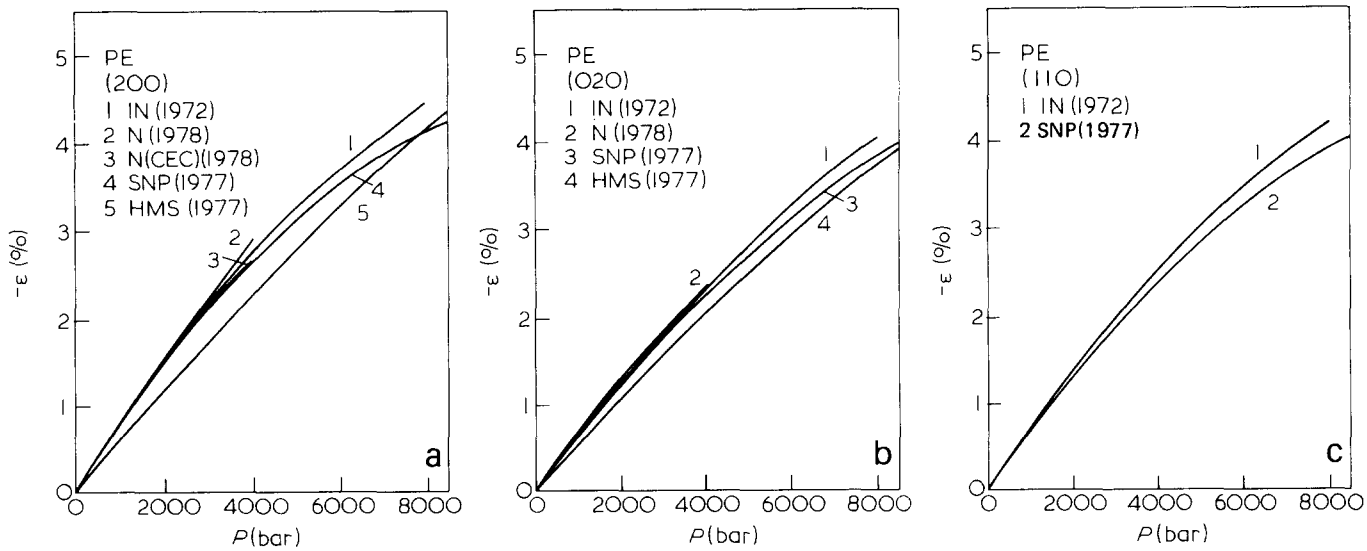

Figure 6 Comparison of the pressure–strain curves for the (200), (020) and (110) *o*-PE planes among various authors. IN, Ito and Nakamura[41,45–46,50]; N, Nakafuku[44]; CEC, chain-extended crystal; SNP, Sham, Newman and Pae[37]; HMS, Hikosaka, Minomura and Seto[38]. Nakafuku's $\epsilon_{(020)}$ data (CEC sample) nearly coincide with the $\epsilon_{(020)}$ obtained by him for a drawn sample shown in (b) with symbol N

where the observed results on the (200) and (110) planes of the unoriented and annealed sample (open and full circles) are compared with those for drawn and oriented samples represented by solid lines calculated from equation (15) for the (200) and equation (20) (below) for the (110) planes.

$$-\varepsilon_{(110)} = 7.69 \times 10^{-6} P - 0.373 \times 10^{-9} P^2 + 0.009 \times 10^{-12} P^3 \qquad (20)$$

$$(P \leqslant 7850 \text{ bar})$$

Despite the large difference expected in the morphology between the unoriented and the drawn and oriented polymer materials, the same strains are observed in the (200) and (110) planes, lending strong support for the assumption of homogeneous stress. Moreover, the results of Ito and coworkers are in complete agreement with the results obtained recently by Nakafuku (4 kbar)[44]. This is shown in *Figure 6*, where data obtained by the diamond anvil technique (Sham, Newman and Pae (14 kbar)[37] and Hikosaka, Minomura and Seto (45 kbar)[38]) are also cited. Although the absolute values of the strain are themselves small, the results obtained by Hikosaka *et al.* are a little too low.

Most authors represent their results for the linear and volumetric strains by third-order polynomials $-\varepsilon_{(hkl)} = AP + BP^2 + CP^3$. Numerical values of A, B and C reported by various authors for *o*-PE crystal are listed in *Table 2*.

To study the effect of the defects induced by chain-branching or foreign side groups on the pressure–strain behaviour of the polyethylene crystal[45,46,50], another HDPE sample (sample 2), an LDPE sample (sample 3) and an ethylene–vinyl alcohol copolymer containing 3.9 mol% OH groups (sample 4) were used. Recrystallized n-heptacosane (n-$C_{27}H_{56}$, sample 5) was prepared as a reference material. These and the HDPE sample used in the preceding section (sample 1) were characterized as shown in *Table 3*.

In *Figures 7a* and *7b*, the strains for the (200) and (110) planes as a function of pressure are compared among these five polyethylene samples. Clearly, the two HDPE samples exhibit similar strains, while samples 3, 4 and 5 show larger strains in the (200) and (110) planes.

Strains in the *b*-axis direction were calculated for samples 3, 4 and 5 from observed values of $\varepsilon_{(200)}$ and $\varepsilon_{(110)}$ using equation (14). These, with addition of some experimental plots for samples 3 and 4, are compared in *Figure 7c* with the observed $\varepsilon_{(020)}$ values for the two HDPE samples. It is found from *Figures 7a*, *7b* and *7c*, that defects clearly increase the compressibility of polyethylene crystal. This is consistent with the theoretical calculations of Tashiro, Kobayashi and Tadokoro[26] who demonstrated that the linear compressibility of *o*-PE crystal increases with increasing cell dimensions. κ_0 values calculated for the *b*-axis direction in the LDPE sample from *Figures 7a*, *7b* and *7c* are listed in *Table 5*.

The coefficients which appear in the polynomial representing the linear crystal strains are, when determined by least squares, fairly sensitive to the experimental errors in the strains. Further, they are inherently variable to some degree in the observed range of applied pressure. Thus, the absolute values and not the differentiated values of the strain are recommended as a safer basis for discussion, particularly for purposes of a strict comparison with theory. The excellent agreement seen in *Table 2* between the results by Ito *et al.* and Nakafuku should be due to the fact that DHPE gives sharp and clear reflections and minimal experimental error in reading the reflection angle.

The bulk compressibility β_T as defined by equation (21) may be deduced as a function of pressure by differentiating the volumetric strain with respect to P:

$$\beta_T = -\frac{1}{V_0}\left(\frac{\partial V}{\partial P}\right)_T \qquad (21)$$

The results for β_T obtained by various authors are compared in *Figure 8*, in which the data by Hatakeyama, Hashimoto and Kanetsuna[47] were obtained by dilatometry using chain-extended 90% crystalline sample

Table 2 Polynomial expressions for the linear and volumetric strains of *o*-PE crystal as function of pressure. Coefficients for $-\epsilon(hkl)$ or $-\Delta V/V_0 = AP + BP^2 + CP^3$ are given. P in bars

(hkl) or $-\Delta V/V_0$	Temperature (K)	Sample preparation[a]	$A \times 10^6$	$B \times 10^9$	$C \times 10^{12}$	$\kappa_0 \times 10^6$	$\beta_0 \times 10^6$	P(max)[b]	Grüneisen parameter[c] (γ)	Author
200	293	DA	11.7	−1.25		11.7		2940		Ito and Marui[15]
020			7.4	−0.20		7.4				
002			0.31	−0.033		0.31				
$-\Delta V/V_0$			19.5	−1.49			19.5		3.4	
200	293	DA	8.77	−0.54	0.018	8.77		7850		Ito and Nakamura[41,45,46,50]
020			6.72	−0.24	0.005	6.72				
002			0.13			0.13				
110			7.69	−0.37	0.009	7.69				
$-\Delta V/V_0$			15.6	−0.84	0.030		15.6		3.0	
200	293	DA	9.03	−0.71	0.074	9.03		3900		Nakafuku[44]
200		CEC	9.29	−0.78	0.034	9.29				
020		DA	6.97	−0.31	0.01	6.97				
020		CEC	6.75	−0.10	−0.02	6.75				
002		DA	0.12			0.12				
$-\Delta V/V_0$		DA	16.13	−1.02	0.085		16.13		3.4	
$-\Delta V/V_0$		CEC	16.15	−0.88	0.008		16.15		2.9	
200	398	DA	16.52	−2.59	0.253	16.52		3900		Nakafuku[44 d]
200	403	CEC	18.52	−2.55	0.194	18.52				
$-\Delta V/V_0$	398	DA	25.63	−3.89	0.389		25.63		5.4	
$-\Delta V/V_0$	403	CEC	25.38	−2.65	0.169		25.38		3.6	
200	298	MA	8.63	−0.553	0.0156	8.63		13 700		Sham, Newman and Pae[37]
110			7.39	−0.401	0.0118	7.39				
020[e]			6.84	−0.334	0.0101	6.84				
$-\Delta V/V_0$			15.88	−1.043	0.0342		15.88		3.6	
200	298	MA	6.25	−0.137	0.0012	6.25		45000		Hikosaka, Minomura and Seto[38]
020			5.55	−0.118	0.0012	5.55				
$-\Delta V/V_0$			12.00	−0.29	0.0030		12.00		(1.5)	

[a] DA, drawn and annealed; CEC, chain-extended crystal, isothermally-crystallized at 5000 kg cm^{-2}; MA, moulded and annealed (unoriented).
[b] Polynomial is valid only below this pressure.
[c] Given by[15] $\gamma = -0.5 - B/A^2$
[d] For (020) and (002), the same values of the coefficient as obtained at 293K are applicable[44].
[e] Calculated from $\epsilon_{(110)}$ and $\epsilon_{(200)}$

of *o*-PE. As shown, β_T for *o*-PE rapidly decreases with increasing pressure and, at ~8 kbar, has reduced to half the initial value $\beta_T(P \to 0)$. This initial β_T, obtained at room temperature, is abbreviated to β_0.

Comparison with theory

Results at room temperature. Müller[17] studied the hydrostatic compression of a polymer crystal both theoretically and experimentally. He calculated the linear compressibilities of paraffin crystals in a direction perpendicular to the chain-axis at absolute zero and obtained two values of 3.8×10^{-6} and 10.8×10^{-6} bar^{-1} by using two different sets of potential functions.

Since Müller, calculations of linear and bulk compressibilities and isothermal P–V relationships have been carried out by many authors. Their computation methods can be divided into two groups: one is based on Born–Huang lattice dynamics[19,65] which predicts the initial compressibilities at $P=0$; the other system uses equation (7), taking the coordinates of the non-bonded atoms in the crystal as force centres which vary as functions of temperature and pressure.

The former calculation method was refined recently by Tashiro, Kobayashi and Tadokoro[25,26] who used the B matrix in the normal coordinate treatments and succeeded in much reducing the number of parameters for computation by introducing space group symmetry of the crystal. The latter type of calculation has been carried out by Müller[17], Brandt[18], Pastine[21], Miyaji[31] and also by Kobayashi[27]. Of these five authors, the first two calculated the 0K compressibility and isotherm, while the last three took into account the contribution of the lattice vibration to provide an equation of state.

For *o*-PE, if the crystal structure at $T=0$ and $P=0$ is known by extrapolation from data at very low temperatures under atmospheric pressure, and if isotropic compression in the transverse direction is assumed together with incompressibility along the chain-axis and conservation of the angle θ between the plane of the zigzag and the *ac*-plane, then the coordinates of the atoms in the crystal at 0K can be predicted as a function of volume. This makes it possible to solve equations (2) and (9) which give the 0K isotherm. So far the zero-point energy has been neglected.

From the 0K isotherm obtained in this way, Pastine has calculated[21] the Grüneisen parameter for the acoustical low frequency vibrations which prevail over the optical high frequency vibrations in contributing to the thermal pressure. He used the equation:

$$\gamma = -\frac{1}{2} - \frac{\frac{1}{2}V(\mathrm{d}^2P/\mathrm{d}V^2!}{(\mathrm{d}P/\mathrm{d}V)} \qquad (22)$$

Equation (22) originates[32] from the Debye theory which describes the frequency of an elastic wave propagating in

Table 3 Characterization of polyethylene samples[45]

No. of sample	Material: Polymer	Grade	Manufacturer	Double bonds per 1000 C: RCH=CHR'	RCH=CH$_2$	RR'=CH$_2$	CH$_3$ per 100 C	Draw ratio	Annealing: Temp. (°C)	Annealing: Time (min)	Density at 30°C (g cm^{-3})	Notes
1	HDPE	Sholex 6050	Showa Denko	0.054	2.20	0.085	0.9	x10	120	180	0.970	$\bar{M}_w = 7.4 \times 10^4$, $\bar{M}_n = 0.84 \times 10^4$
2	HDPE	Sholex 6009	*Ibid.*	0	2.51	0.088	0.3	x8	120	180	0.967	$\bar{M}_w = 12.0 \times 10^4$, $\bar{M}_n = 0.86 \times 10^4$
3	LDPE	Yukalon LK-30	Mitsubishi Yuka	0.120	0.26	0.69	5.5	x4	90	180	0.911	$\bar{M}_n = 1.10 \times 10^4$
4	Ethylene–vinyl alcohol copolymer	Nipoflex 540*	Toyo Soda					x5	90	180	0.936	Contained 3.9 mol % of –OH side group
5	n-Heptacosane	E.P.	Tokyo Chemicals						50	300		Recrystallized from toluene solution, M.p. 59.6–61.2°C

* Commercial name of an ethylene–vinyl acetate copolymer manufactured by Toyo Soda Manufacturing Co. Sample 4 was obtained by complete saponification of this polymer

an isotropic continuum as a function of volume, volumetric compressibility and density. Applying the Debye-like frequency distribution, where all the vibrations are assumed to have the same γ as that determined by equation (22), Pastine evaluated the thermal contribution to the pressure by the following equation,

$$P_T = \frac{\rho_0 2nfkT\gamma}{x} \times 3\left(\frac{T}{\theta}\right)^3 \int_0^{\theta/T} \frac{z^3}{e^z - 1} dz \qquad (23)$$

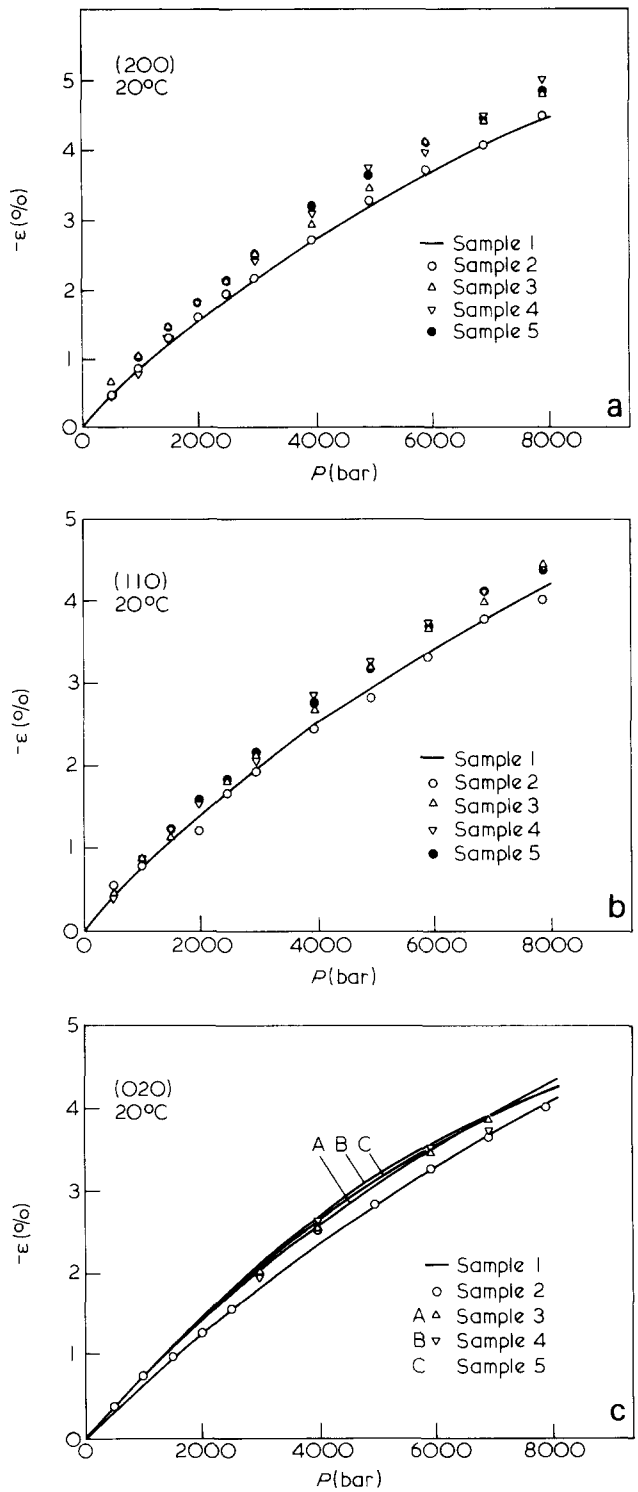

Figure 7 Pressure–strain plots for (200), (110) and (020) planes of LDPE, ethylene–vinyl alcohol copolymer and n-heptacosane compared with HDPE. The numbers refer to the text and *Table 3*

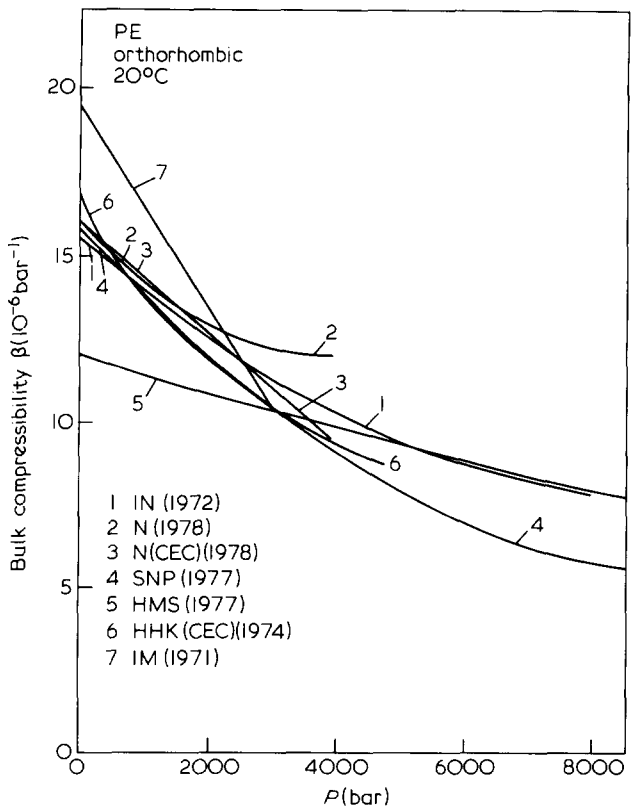

Figure 8 Dependence of $\beta_{20-25°C}$ on pressure for *o*-PE crystal reported by various authors. IN, Ito and Nakamura[41,45,46,50]; N, Nakafuku[44]; CEC, chain-extended crystal; SNP, Sham, Newman and Pae[37]; HMS, Hikosaka, Minomura and Seto[38]; HHK, Hatakeyama, Hashimoto and Kanetsuna[47]; IM, Ito and Marui[15]

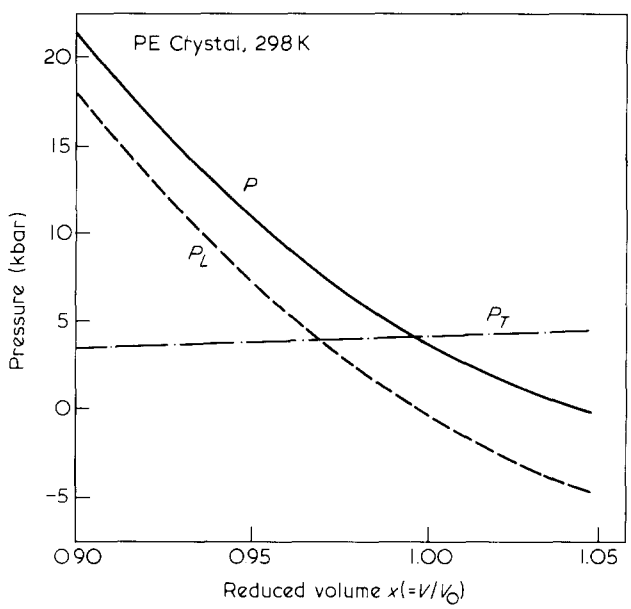

Figure 9 Calculated results[21] for pressure (P), lattice pressure (P_L) and thermal pressure (P_T) for *o*-PE crystal as a function of reduced volume. V_0 is the specific volume at $P = 0$ and $T = 0$

where ρ_0 is the density at $P=0$ and $T=0$; n is the number of atoms; $2n$ is the number of degrees of freedom for the acoustical vibration, of which a further fraction of $2nf$ was assumed to contribute to the thermal pressure ($f=0.278$ at 298K); x is the reduced volume given by $x=V/V_0$ where V_0 is the specific volume at $P=0$ and $T=0$. θ is the Debye temperature—123K was employed for *o*-PE crystal. The calculated P_L (equation 9) which does not depend on temperature, P_T at 298K and $P=P_L+P_{T=298K}$ are shown in *Figure 9* as a function of x. At $x=1.0473$—the value at $P=0$ and $T=298$K for *o*-PE crystal—P_L amounts to -4.57 kbar which equilibrates with $P_T=+4.57$ kbar. Because P_T varies much more slowly than P_L, the volumetric compressibility β_T is primarily determined by the variation in P_L. Pastine's treatment was later applied by Miyaji[31] to polyoxymethylene crystal. He estimated that at 298K P_T amounts to 4.7 and 3.35 kbar at $P=0$ and 20 kbar, respectively.

Recently, Kobayashi[27,29] refined Pastine's treatment using a novel treatment. For each particular set of lattice constants, he calculated the normal frequencies of the **k** vectors in the first Brillouin zone of the reciprocal space at intervals of 2.25° for δ_c and 4.5° for δ_a and δ_b (where δ_c, δ_a and δ_b represent, respectively, the phase differences in vibrations in the neighbouring unit cell along the *c*-, *a*- and *b*-axes). Thus for a given temperature and given structural parameters, namely, a, b and the setting angle θ (c assumed constant) then the Helmholtz free energy and the pressure associated with it can be calculated from equations (1)–(6). Kobayashi found the contribution from the zero point energy, which had been neglected by the other authors, was not negligible.

As an example of his calculations, the calculated pressure at $T=300$K and $\theta=48.8°$, expressed in a two-dimensional manner with a and b as variables, is shown in *Figure 10*. Full curves represent isobars in the 10^3 atm interval, while the broken loops represent the Helmholtz free energy per mole of CH_2 at $P=0$ with an interval of 10 J. The minimum in the Helmholtz free energy at $P=0$ gives $a=7.508$ and $b=5.184$ Å. Along each isobar, the Gibbs free energy $G=A+PV$ has been calculated and gives a minimum at the position indicated by a cross, indicating that a and b should decrease with increasing pressure. As shown in *Figure 10*, the minimum G criterion

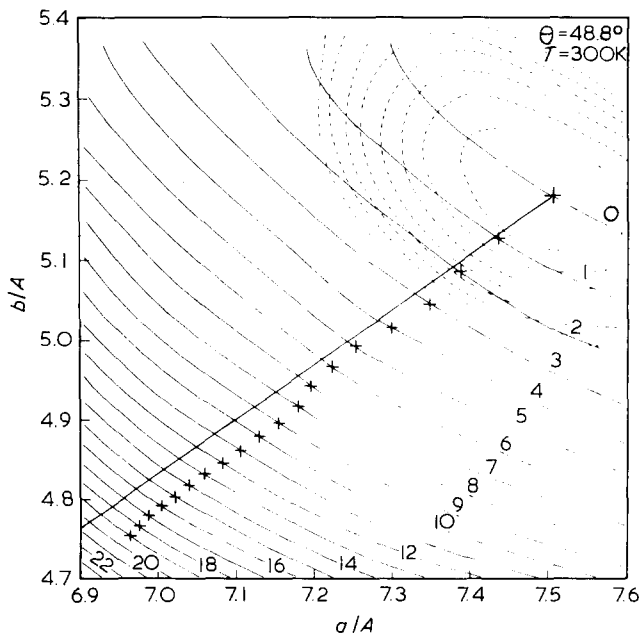

Figure 10 Isobar lines for *o*-PE crystal (θ = 48.8°) at 300K (Kobayashi[27]). ——, Isobar lines at the pressures indicated (unit, 1.013 kbar = 10^3 atm); – – – –, contour map of Helmholtz free energy drawn at intervals of 10 J mol^{-1} per CH_2; +, the Gibbs free energy minima. The straight line starting from a = 7.508 Å, b = 5.184 Å indicates isotropic contraction with a/b = constant

predicts an anisotropic compression which deviates slightly from the isotropic compression (represented by a thick solid straight line) towards the side which favours more compressibility in the *b*-axis direction. Assuming incompressibility along the *c*-axis, the volume corresponding to the *G*-minimum position can be calculated to give the volumetric strain, $-\Delta V/V_0$, at $T=300$K, without assuming the isotropic lateral compression used by the other authors.

The results are shown in *Figure 11*, where the case $\theta=42°$ is also given. It is seen that the calculations by Kobayashi are in good agreement with the values observed by Ito and Nakamura[45,46] and by Nakafuku[44]. In *Figure 11* are also given the calculations by Pastine[21] and the observed data by Hikosaka, Minomura and Seto[38] and by Sham, Newman and Pae[37]. The observed results were drawn using polynomials reported by these authors to describe $-\Delta V/V_0$ (*Table 2*).

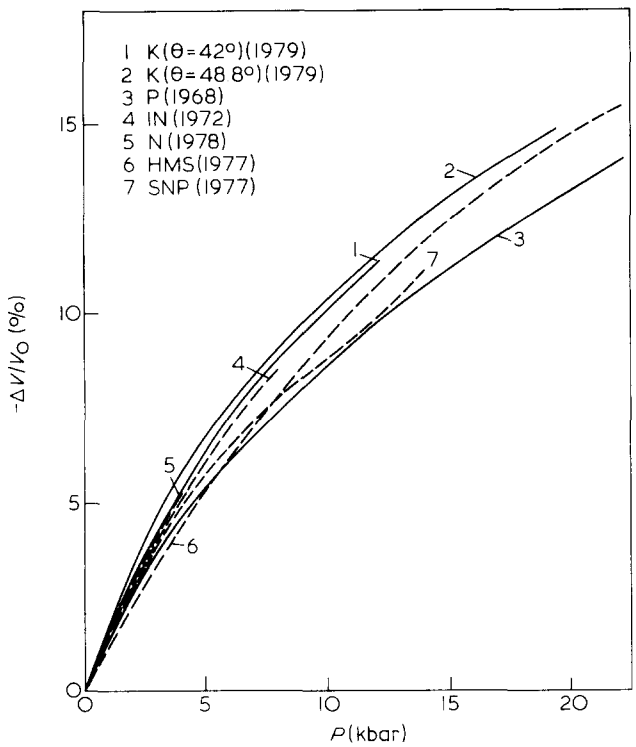

Figure 11 Calculated (——) and observed (— — —) volumetric strain vs. pressure. K, Kobayashi[27]; P, Pastine[21]; IN, Ito and Nakamura[41,50]; N, Nakafuku[44]; HMS, Hikosaka, Minomura and Seto[38]; SNP, Sham, Newman and Pae[37]

It should be pointed out that the polynomial formula reported by Hikosaka *et al.* fails below 8 kbar to fit the i.r. experimental data[38], namely, $-\Delta V/V_0(\%)=4.130$, 4.935, 7.626, 7.202 and 8.431 at pressures 2.65, 3.75, 6.80, 6.85 and 8.25 kbar, respectively. These, in turn, were found to be in good agreement[41] with the results obtained by Ito and Nakamura and by Nakafuku. It may be argued, from *Figure 11*, that Pastine's calculation underestimates the compressibility of *o*-PE by about 10% compared with the observed values. In Kobayashi's calculations, a little closer agreement with the experimental results is seen to be obtained at $\theta=42°$.

The Grüneisen parameters for *o*-PE crystal at $P=0$, experimentally obtained and calculated according to equation (22), are listed in *Table 2*. They were found to take a value of ~3.0 at room temperature.

It should be noted at this stage that excellent agreement has been found between the theoretical predictions of Goel, Nanda and Jain[28] and the experimental results obtained by Ito and Nakamura.

The anisotropy of the linear compressibilities along the *a*- and the *b*-axes, predicted in *Figure 10* by Kobayashi from the *G*-minimum criterion, are in the reverse order to the experimental results described in the preceding section. The reason for this discrepancy was attributed by Kobayashi to possible gradual variation of the setting angle θ as the crystal was pressurized. The experimental anisotropy which persists from the initial stages of pressurization (*Figure 3*) can only be explained if the insisted rotation of the setting angle increases[27] and occurs soon after the start of compression to an extent which permits a switching of the anisotropy.

Alternatively, using Born's dynamical theory of the crystal lattice, the experimental anisotropy observed in the transverse linear compressibilities of *o*-PE crystal can also be explained. According to this theory, the elastic constants describing the elastic wave in an anisotropic continuum can be expressed in terms of Born's force constants, which in turn are obtained by taking second derivatives of the interatomic potential energy functions[19]. The calculated elastic compliances for *o*-PE crystal obtained by Odajima and Maeda[19], Wobser and Blasenbrey[23] and Tashiro, Kobayashi and Tadokoro[26] are listed in *Table 4*. For an orthorhombic structure, the results listed in *Table 4* can be extended[26] according to equation (24):

$$\kappa_0(0)=(S_{11}+S_{12}+S_{13})\cos^2\theta+(S_{21}+S_{22}+S_{23})\sin^2\theta. \quad (24)$$

Table 4 Calculated anisotropic elastic compliances and initial linear and volumetric compressibilities (10^{-12} cm^2 dyn^{-1})

Temp. (K)	S_{11}	S_{12}	S_{13}	S_{22}	S_{23}	S_{33}	κ_a	κ_b	κ_c	β_0	Author
77	14.7	−3.3	−0.1	10.9	−0.23	0.40	11.3	7.4	0.07	18.8	Odajima and Maeda[19] *
293	21.4	−2.7	−0.15	12.0	−0.25	0.40	18.5	9.0	0.00	27.6	
77	12.5	−4.2	−0.07	10.7	−0.22	0.40	8.2	6.3	0.11	14.7	Odajima and Maeda[19] †
293	17.4	−4.0	−0.10	11.8	−0.23	0.40	13.3	7.6	0.06	20.9	
0	10.5	−6.223	−0.0046	11.69	−0.095	0.309	4.27	5.37	0.209	9.85	Wobser and Blasenbrey[23]
293	14.48	−4.78	−0.02	11.67	−0.06	0.32	9.68	6.83	0.24	16.75	Tashiro, Kobayashi and Tadokoro[26]

* Calculated for Set I[19] potential functions.
† Calculated for Set III[19] potential functions.

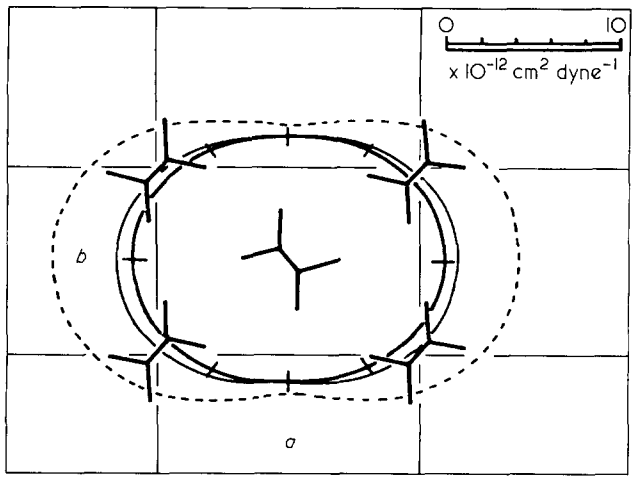

Figure 12 Anisotropy of linear compressibility in the *ab* plane of *o*-PE at 293K (Tashiro *et al.*[26]). ——, Calculated by Tashiro, Kobayashi and Tadokoro[26]; — — —, calculated by Odajima and Maeda[19]; ——, observed by Ito and Nakamura[41,50] (small bars indicate experimental error)

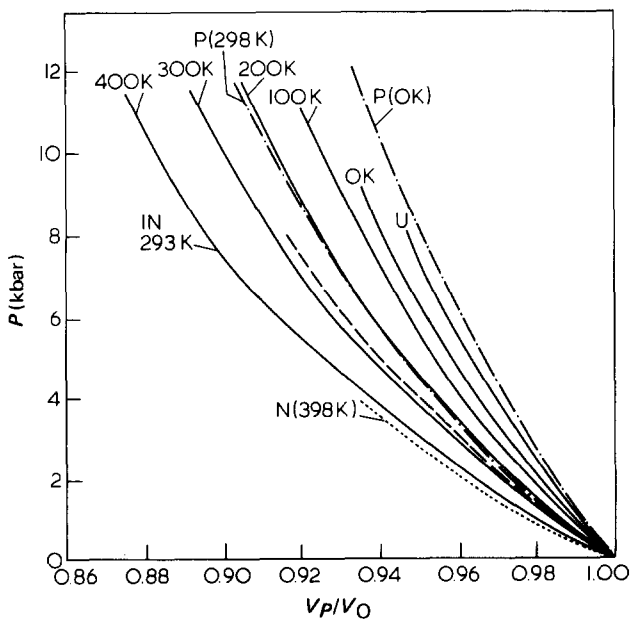

Figure 13 Calculated and observed isotherms for *o*-PE at various temperatures indicated (Kobayashi[27]). ——, Calculated by Kobayashi[27] (*a*/*b* = constant), — · —, calculated by Pastine[21] (*a*/*b* = constant); — — —, observed by Ito and Nakamura[41,50]; · · · · ·, observed by Nakafuku[44]

The results were represented by Tashiro *et al.*[26] on the *o*-PE *ab*-plane by travelling a distance proportional to κ_0 in both directions along the plane normal drawn through the centre of the structure (*Figure 12*).

The anisotropy deduced from Born's lattice dynamics is essentially in agreement with the experiment. In particular, the results calculated by Tashiro *et al.* are in excellent agreement with experiment.

Effect of temperature. The equation of state for the polymer crystal was studied by Pastine[21], Kobayashi[27], Midha and Nanda[24] and Goel, Nanda and Jain[28]. Since the lattice pressure P_L in equation (8) does not depend on temperature, the dependence of P–V relationship on temperature is determined by the ZE pressure as well as the thermal pressure.

Theoretical isotherms with $\theta = 42°$ at 0, 100, 200, 300 and 400K were obtained by Kobayashi (*Figure 13*) where isotropic transverse compression was assumed. At 400K, Kobayashi's calculations gave fairly good agreement with the results recently obtained by Nakafuku[44]. In *Figure 13*, the *U*-isotherm was calculated at 0K ignoring ZE and it is clear that the contribution of P_{ZE} compared with P_L is not negligible. Since Pastine's 0K isotherm comes close to Kobayashi's *U*-isotherm, the main reason for Pastine's underestimation may be ascribed to his ignoring the ZE contribution.

Theoretical calculations of temperature dependence for the linear strain are still not available[102]. Experimental results obtained by Nakafuku[44], however, cover the pressure range 1–3900 bar and the temperature range 293–403K. Of the principal axes linear strains ε_a, ε_b, ε_c, unique and interesting behaviour was revealed for ε_a. The three polynomial coefficients A_a, B_a and C_a are recorded as a function of temperature in *Figure 14*, where two samples of HDPE (a drawn material and a chain-extended crystal) were used. A_a, which equals $\kappa_{0,a}$, is almost constant until the temperature reaches 70°C, when it exhibits an abrupt and steep increase to above 120°C; a shoulder is observed at ~100°C. This shoulder was

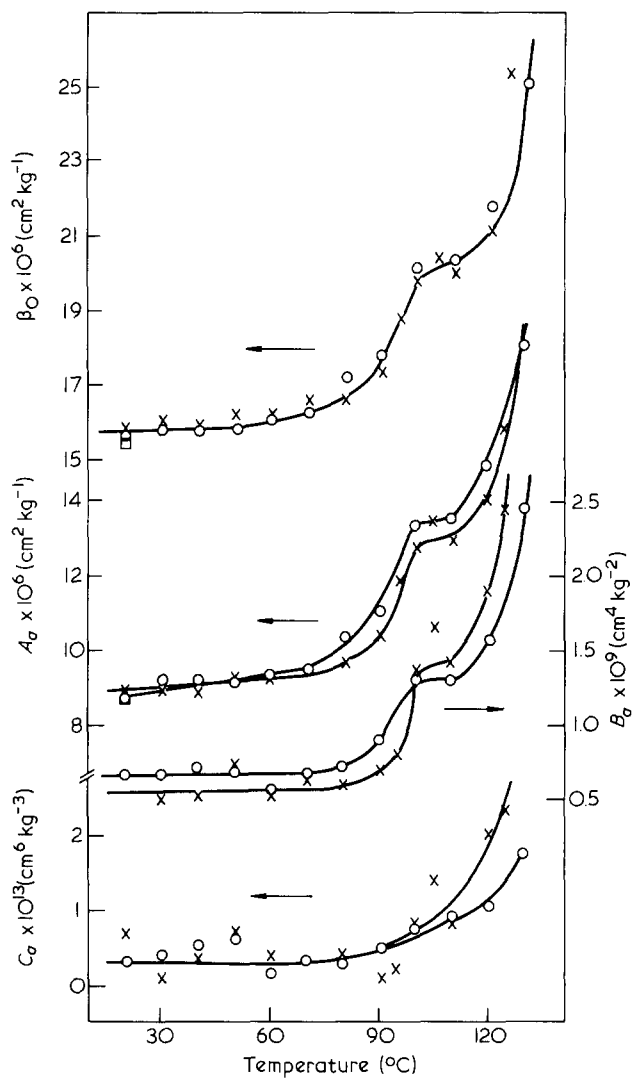

Figure 14 Variation of A_a, B_a and C_a with temperature, and temperature dependence of β_0 for *o*-PE (Nakafuku[44]). X, Drawn HDPE; ○, CEC of HDPE. All the polynomial coefficients with respect to (020) and (002) planes (A_b, B_b, C_b; A_c) were constant and independent of temperature[44]

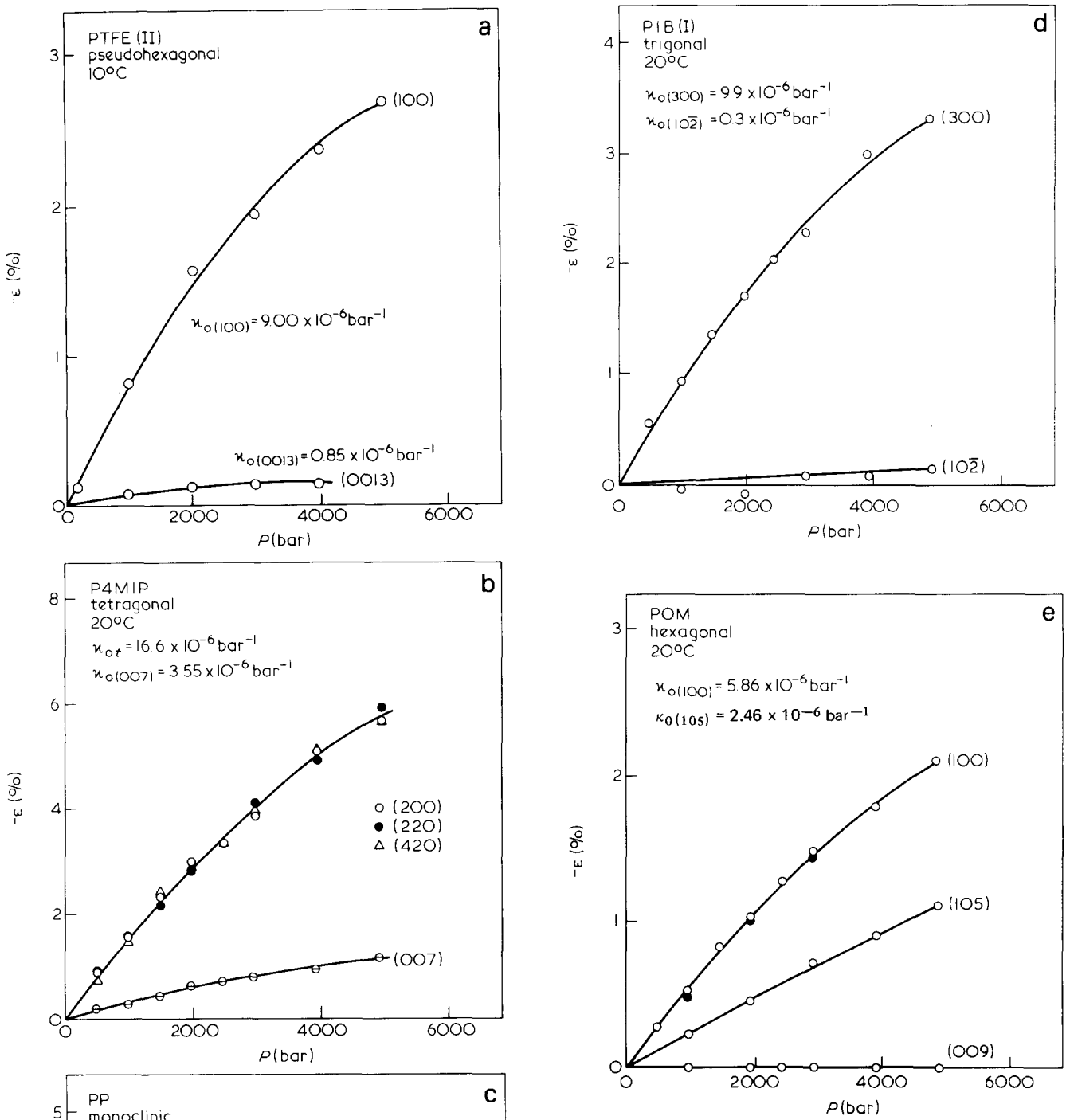

Figure 15 Pressure–strain curves for (a) PTFE(II); (b) it-P4M1P; (c) it-PP; (d) it-P1B(I); and (e) POM

ascribed by Nakafuku to crystalline dispersion. Over this temperature range $\kappa_{0,b}$ and $\kappa_{0,c}$ are essentially constant, and the temperature dependence of the bulk compressibility β_0 is primarily determined by $\kappa_{0,a}$, as shown in *Figure 14*[44].

Nakafuku also demonstrated that the Grüneisen parameter remained constant up to ~90°C; above 90°C, it increased with increasing temperature. A steeper dependence on temperature was found for drawn HDPE than for the CEC sample (*Table 2*).

The unique temperature dependence of ε_a and $\kappa_{0,a}$ of *o*-PE presents a problem for future study.

POLYMERS WITH HELICAL OR CONTRACTED SKELETONS

Polytetrafluoroethylene

According to recent investigations by Nakafuku and Takemura[42], the chain molecule in the PTFE crystal, which under normal pressure has a helical 13_6 conformation (phase II) or a slightly untwisted form of 15_7 (phase IV)[66,67], takes the fully-extended planar zigzag structure under high pressure (phase III). It is clear that upon transition to the high-pressure phase, the crystal of PTFE elongates along the fibre-axis and contracts laterally, the net effect being the observed decrease in volume[68].

It is interesting to enquire whether the helical PTFE chain elongates or contracts along the fibre-axis during pressurization. Results obtained at 10°C in the phase II state are given[52] in *Figure 15a*, where the strains in the (0013) plane are the longitudinal strains along the fibre-axis, while those in the (100) plane are the transverse strains. Clearly, the helical PTFE chain contracts with increasing pressure, and, probably, this effect continues until the transition to the high pressure phase arises, when the chain abruptly untwists into the fully-extended planar zigzag structure. The strain $\varepsilon_{(100)}$ at 4903 bar, -0.0274, is almost the same as $\varepsilon_{(020)}$ of *o*-PE at the corresponding pressure. In *Figure 15a*, the solid line is a second order polynomial representation obtained by the least squares method. The coefficients determined there will be summarized and discussed in *Table 5*.

Isotactic poly(4-methyl-1-pentene)

For an ordinary organic molecular crystal containing no extra heavy atoms, a strong correlation between volumetric compressibility, β_0, and crystal density can be expected. β_0 increases with decreasing density because of the resulting increase in unoccupied space in the structure: thus compressibility increases.

Of polymer crystals with low density, it-P4M1P is a unique example, exhibiting a crystalline density[69] (0.812 g cm^{-3}) lower than that of the noncrystalline region[70] (0.838 g cm^{-3}). The chain molecule in the it-P4M1P crystal assumes a helical conformation[69,71], $13.85/7_2/86.8$, where 13.85 denotes the fibre period (Å), 7_2 a helix with seven repeating units per two turns and 86.8 the cross-sectional area per chain ($Å^2$). The degree of packing of the molecules may be expressed in terms of the packing density[72], k, as defined by equation (25):

$$k = zv_0/v \tag{25}$$

where z is the number of chains per unit cell, v_0 the volume of the chain by framing it with the van der Waals radii of the constituent atoms and with sections of the six walls of the unit cell, and v is the unit cell volume. The k value estimated[73] for the tetragonal crystal of it-P4M1P is 0.57, an unusually small value compared with k for *o*-PE[73] of 0.70. Results given in *Figures 15b* and *16* were obtained by the following formulae ($P \leqslant 4900$ bar)[49,50,54]:

$$-\varepsilon_t = 16.6 \times 10^{-6} P - 1.01 \times 10^{-9} P^2 \tag{26}$$

$$-\varepsilon_{(007)} = 3.55 \times 10^{-6} P - 0.25 \times 10^{-9} P^2 \tag{27}$$

$$-\Delta V/V_0 = 36.7 \times 10^{-6} P - 2.7 \times 10^{-9} P^2 \tag{28}$$

where ε_t in equation (26) refers to the mean value of ε in the transverse direction. In *Figure 15b* it is clear that the linear compressive strains in the transverse direction are isotropic and the tetragonal structure of it-P4M1P at atmospheric pressure is preserved under high pressures. The mean value of κ_0 in the transverse direction, $\kappa_{0,t}$, and β_0 were found to be 16.6×10^{-6} and 36.7×10^{-6} bar^{-1}, respectively. These linear and volumetric compressibilities are as large as expected, more than twice as large as those for *o*-PE. They will be discussed in *Table 5*.

The 007 reflections appearing in *Figure 16* indicate the longitudinal strain along the fibre-axis induced by hydrostatic pressure, $\varepsilon_l (= \varepsilon_c)$, which reached (in *Figure 15b*) -0.011 at 4900 bar. This value of ε_l may be explained[74] using equation (29):

$$\varepsilon_l = -\frac{(1-2\nu)}{E_l} P \tag{29}$$

where ν is the mean Poisson ratio, given by $\nu = (\nu_{12} + \nu_{13})/2$; P is the pressure and E_l is the Young's modulus along the fibre-axis. E_l for it-P4M1P was found by Sakurada and Kaji[11] to be 6.6×10^4 bar. The Poisson ratio for the tetragonal it-P4M1P crystal is not known and $\nu = 0.43$ was assumed.

Isotactic polypropylene, isotactic poly(1-butene) (I) and polyoxymethylene

The chain structures for these three polymers which all exhibit helical skeleton conformations in the crystalline state are: $6.50/3_1/34.4$; $6.50/3_1/45.2$; and $17.39/9_5/17.3$ for it-PP[75], it-P1B(I)[76] and POM[77], respectively. The force constants for the internal rotation are smaller by approximately one order of magnitude than those for the bond-angle deformation and by approximately two orders of magnitude than those for the bond stretching deformation[78]. Since the mechanism of internal rotation is assumed to occur in longitudinal deformation of an isolated chain, the polymer crystal will have low Young's moduli, if free untwisting of the chain is permitted during stretching. E_l values for it-PP, it-P1B(I) and POM found by Sakurada, Ito and Nakamae[10] and Sakurada and Kaji[11] are 34×10^4, 24.5×10^4 and 53×10^4 bar, respectively, one fifth to one tenth of E_l for *o*-PE,[10,11] ($= 235 \times 10^4$ bar). The previously mentioned value of E_l for it-P4M1P is 1/36 of E_l for *o*-PE. Such low values of E_l found for the crystals of it-PP, it-P1B(I), POM and it-P4M1P have been theoretically explained[79].

Under hydrostatic pressure, the fibre-axial strain should obey equation (29). However, no systematic information about the Poisson's ratio of the polymer crystal, theoretical or experimental, is available. The experimental results[46,49,50] for the strains obtained under the hydrostatic pressure are shown in *Figures 15c–15e*. In these Figures, the strain obtained from the 009 reflection of POM gives ε_l, while, for it-PP and it-P1B, no reflection could be found to represent ε_l directly. The angles between the fibre-axis and the normal plane for $(\bar{1}13)$ of it-PP and $(10\bar{2})$ of it-P1B(I) are 10.8° and 12.0°, respectively, and the strains in these two planes give approximate values of ε_l. ε_l may be calculated from the observed spacings obtained under different pressures for one ***hkl*** reflection on the *l*th layer line and two *hk*0 reflections on the equator. Values of ε_l obtained in this manner are highly sensitive to experimental errors in $\varepsilon_{(hkl)}$ or $\varepsilon_{(hk0)}$ because ε_l itself is

Table 5 Linear and bulk compressibilities for various polymer crystals

Polymer, crystal system[a]	Crystal density ρ_{cryst} (g cm^{-3})	Packing density, k	Lattice plane (hkl),[b] $-\Delta V/V_0$	Polynomial coefficients[c] $A \times 10^6$	$B \times 10^9$	$C \times 10^{12}$	Max. pressure[d] (bar)	$\kappa_0 \times 10^6$	$\beta_0 \times 10^6$	Pressure transmitting medium[e]	Reference
it-P4M1P tetragonal	0.812	0.57	200	17.0	–1.13	–	4900	17.0		Water	49,50,54
			220	16.1	–0.843	–		16.1			
			420	16.7	–1.06	–		16.7			
			007	3.55	–0.251	–		3.55			
			$-\Delta V/V_0$	36.7	–2.7	–			36.7		
it-PP monoclinic	0.938	0.66	110	8.45	–0.523	–	4900	8.45		Water	46,49,50
			040	12.2	–0.871	–		12.2			
			100*	8.09	–0.490	–		8.09			
			$\bar{1}13$	0.4	–	–		0.4			
			$-\Delta V/V_0$	20.7	–1.47	–			20.7		
			040	11.07	–0.79	0.02	4740	11.07		Silicone oil	53
			100*	7.87	–0.71	0.049		7.87			
n-Heptacosane orthorhombic	0.9425	(0.66)	110	8.99	–0.541	0.014	7850	8.99		Water	45,50
			200	11.1	–0.901	0.036		11.1			
			010*	8.06	–0.381	0.0051		8.06			
			$-\Delta V/V_0$	(19.3)[f]	(–1.37)[f]	(0.05)[f]			(19.3)[f]		
it-P1B(I)	0.951	0.66	300	9.92	–0.647	–	4900	9.92		Water	50
			$10\bar{2}$	0.3	–	–		0.3			
			$-\Delta V/V_0$	20.2	–1.4	–			20.2		
LDPE orthorhombic	0.997	0.70	110	8.94	–0.625	0.027	7850	8.94		Water	45,46,50
			200	11.3	–1.11	0.060		11.3			
			010*	7.90	–0.407	0.012		7.90			
			$-\Delta V/V_0$	19.3	–1.61	0.086			19.3		
HDPE orthorhombic	1.008	0.70	110	7.69	–0.373	0.009	7850	7.69		Water	41,45,46,49,50
			200	8.77	–0.540	0.018		8.77			
			020	6.72	–0.235	0.005		6.72			
			310	9.42	–0.786	0.038		9.42			
			002	0.13	–	–		0.13			
			$-\Delta V/V_0$	15.6	–0.84	0.030			15.6		
Adamantane cubic ($P \leq 4700$ bar)	1.07	0.67	200	8.16	–0.550	–	4700	8.16		Water	46,49
			$-\Delta V/V_0$	24.3	–1.85	–			24.3		
tetragonal ($P \geq 4700$ bar)			110	3.50[g]	–0.238[g]	–	7850	3.50[h]		Water	46,49
			001	5.23[g]	–0.207[g]	–		5.23[h]			
			$-\Delta V/V_0$	12.2[g]	–0.49[g]	–			12.2[h]		
PTMO(I)	1.112	0.70	110	9.7	–0.42	–	4900	9.7		Silicone grease	46
			020	8.3	–0.45	–		8.3			
			$\bar{2}25$	1.6	–0.062	–		1.6			
			3110	~0							
			$-\Delta V/V_0$	17.8	–0.99	–			17.8		
Ny-6(γ) monoclinic (b)	1.163	0.707	200	16.3	–0.80	–	5880	16.3		Ethyl alcohol	41,50,58
			$20\bar{2}$	3.79	–0.24	–		3.79			
			001	4.60	–0.13	–		4.60			
			$-\Delta V/V_0$	17.9	–0.42	–			17.9		

cont.

Table 5 – cont.

Polymer, crystal system[a]	Crystal density ρ_{cryst} (g cm^{-3})	Packing density, k	Lattice plane (hkl),[b] $-\Delta V/V_0$	Polynomial coefficients[c] $A \times 10^6$	$B \times 10^9$	$C \times 10^{12}$	Max. pressure[d] (bar)	$\kappa_0 \times 10^6$	$\beta_0 \times 10^6$	Pressure transmitting medium[e]	Reference
PEO(I) monoclinic	1.228	0.72	110	6.88	–0.611	–	4500	6.88		n-Pentane	41,55
			120	5.82	–0.228	–		5.82			
			$\bar{2}07$	0.99	+0.561	–		0.99			
			100*	7.60	–0.87	–		7.60			
			010*	4.08	+0.40	–		4.08			
			001*	0.6	–	–		0.6			
			$-\Delta V/V_0$	11.7	–0.32	–			11.7		
Ny-6(α) monoclinic (b)	1.235	0.750	200	2.58	–0.036	–	4900	2.58		Ethyl alcohol	41,50,58
			002	10.5	–0.68	–		10.5			
			$-\Delta V/V_0$	13.1	–0.74	–			13.1		
Hexamethylene tetramine cubic	1.345	0.72	112	3.91	–0.127	–	4900	3.91		n-Heptane	41,50
			$-\Delta V/V_0$	11.7	–0.43	–			11.7		
at-PVA monoclinic (b)	1.350	0.77	200	4.56	–0.15	–	5880	4.56		n-Pentane	58
			002	7.14	–0.32	–		7.14			
			101	7.10	–0.25	–		7.10			
			$10\bar{1}$	5.02	–0.13	–		5.02			
			$20\bar{1}$	4.3	–0.18	–		4.3			
			$-\Delta V/V_0$	11.7	–0.48	–			11.7		
PEOB(α) orthorhombic	1.391	–	200	7.03	–0.152	–	4900	7.03		Water	41,51,56
			110	6.58	–0.257	–		6.58			
			010*	6.49	–0.279	–		6.49			
			006	0.24	–	–		0.24			
			$-\Delta V/V_0$	13.8	–0.48	–			13.8		
Pentaerythritol tetragonal	1.396	0.7	200·112	1.98	–0.087	–	4900	1.98		n-Pentane	50
			101	2.77	–0.079	–		2.77			
			002·110	5.88	–0.45	–		5.88			
			001*	4.39	–0.060	–		4.39			
			$-\Delta V/V_0$	8.34	–0.17	–			8.3		
PET triclinic	1.455	0.75	100	9.97	–0.53	–	5880	9.97		Water	94
			010	4.88	–0.097	–		4.88			
			$\bar{1}05$	0.73	0.000	–		0.73			
			001*	1.20	–0.026	–		1.2			
			$-\Delta V/V_0$	16.1	–0.69	–			16.1		
POM hexagonal	1.491	0.78	100	5.86	–0.326	–	4900	5.86		Glycerol–methyl alcohol (1 : 1)	41,49,50
			105	2.46	–0.0466	–		2.46			
			009	~0							
			$-\Delta V/V_0$	11.7	–0.686	–			11.7		
			100					5.5		Ethyl alcohol (25°C)	31
			009					0.15			
PVDF(II) monoclinic ($\beta = 90°$)	1.925	–	200	5.39	–0.33	–	5880	5.39		Water	60
			110	5.29	–0.23	–		5.29			
			120	5.45	–0.23	–		5.45			
			130	5.69	–0.36	–		5.69			
			002	0.27	–0.0036	–		0.27			

cont.

Table 5 – cont.

Polymer, crystal system[a]	Crystal density ρ_{cryst} (g cm^{-3})	Packing density, k	Lattice plane (hkl),[b] $-\Delta V/V_0$	Polynomial coefficients[c] $A \times 10^6$	$B \times 10^9$	$C \times 10^{12}$	Max. pressure[d] (bar)	$\kappa_0 \times 10^6$	$\beta_0 \times 10^6$	Pressure transmitting medium[e]	Reference
PVDF(II) (cont.)			021	3.19	–0.17	–		3.19			
			010*	5.89	–0.38	–		5.89			
			$-\Delta V/V_0$	11.6	–0.75	–			11.6		
			100*					11.4		Silicone oil	100
			110					10.1			
			002					1.3			
			021					4.3			
			200					5.8		Silicone oil	101
			010*					5.9			
			002*					0.76			
			$-\Delta V/V_0$						12.6		
PVDF(I) orthorhombic	1.973	0.84	200·110	5.71	–0.16	–	5880	5.71		Water	60
			020·310	5.61	–0.21	–		5.61			
			001	0.48	–0.077	–		0.48			
			111·201	1.57	–0.047	–		1.57			
			$-\Delta V/V_0$	11.8	–0.48	–			11.8		
			010*					4.3		Silicone oil	100
			111·201					1.4			
			200·110					4.7		Silicone oil	101
			$-\Delta V/V_0$						10.2		
Carbon fibre hexagonal	2.27	0.887	002	3.04	–0.033	–	7850	3.04		Glycerol–water (1 : 1)	41,45,50
			$-\Delta V/V_0$	3.04	–0.033	–			3.04		
Graphite hexagonal	2.27	0.887	002	3.26	–0.074	–	7850	3.26		Glycerol–water (1 : 1)	41,45,50
			$-\Delta V/V_0$	3.26	–0.074	–			3.26		
PTFE(IV)[i] 24°C trigonal	2.302	0.78	100	11.9	–1.15	–	4900	11.9		Water	41,50,52
			0015	1.13	–0.12	–		1.13			
			$-\Delta V/V_0$	25.0	–2.56	–			25.0		
PTFE(II) 10°C pseudo-hexagonal	2.347	0.80	100	9.00	–0.707	–	4900	9.00		Water	41,50,52
			0013	0.85	–0.10	–		0.85			
			$-\Delta V/V_0$	18.9	–1.59	–			18.9		

[a] Case where b-axis instead of c-axis is taken as the fibre-axis is noted by adding (b) after the system description.
[b] Results obtained by calculation from strain data for other planes are denoted with asterisk.
[c] A, B and C are the coefficients for the polynomial formula, $-\epsilon_{(hkl)}$ or $-\Delta V/V_0 = AP + BP^2 + CP^3$, P in bars. A second order polynomial was employed for most cases. Very small strains were expressed by a linear function.
[d] Polynomial expression is valid only below this pressure.
[e] Used in the X-ray diffraction vessel.
[f] Measurement in the c-axis direction was unsuccessful. Data for HDPE, $-\epsilon_{c\text{-axis}} = 0.13 \times 10^{-6} P$ was assumed. However, this must be an underestimation for n-heptacosane crystals because the end-to-end packing of the chains is supported only by weak van der Waals attractions.
[g] As a function of $(P - 4700)$.
[h] Linear and bulk compressibilities at $P = 4700$.
[i] Judging by the phase diagram of PTFE crystal[42], the IV → II phase transition should have occurred in the initial stages of pressurization. This could not be detected in the zero layer photograph.

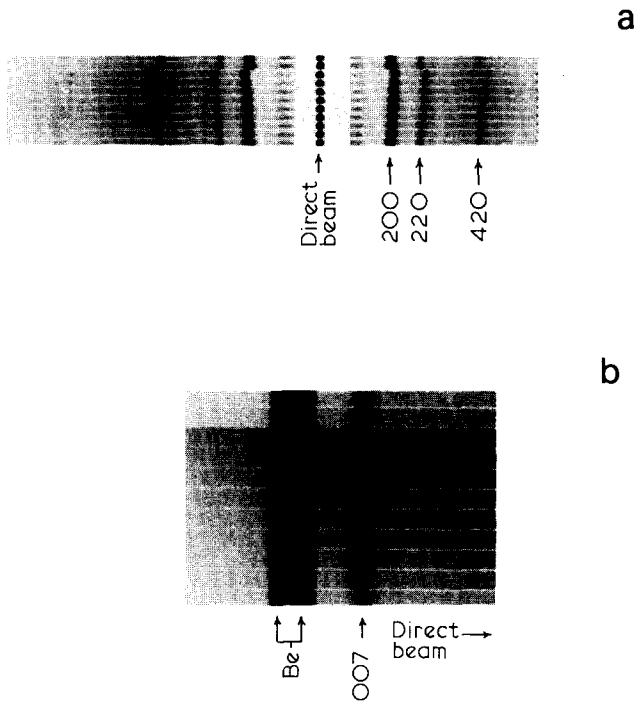

Figure 16 X-ray photographs of (a) the equatorial and (b) the basal 007 reflections of drawn and annealed it-P4M1P. Under pressures of (kg cm^{-2}) (from): 1, 500, 1000, 1500, 2000, 2500, 3000, 4000, 5000, 1 and 138 (a) or 94 (b). Pressure medium, water

small, often comparable in order of magnitude with the experimental errors for $\varepsilon_{(hkl)}$ or $\varepsilon_{(hk0)}$.

As seen from *Figures 15c–15e*, the fibre-axial or the nearly fibre-axial strains found for it-PP, it-P1B(I) and POM are unusually small, in contrast to the results of uniaxial stretching[10,11]. For POM, ε_l is virtually zero even under the highest pressure applied. The same result for $\varepsilon_{(009)}$ in POM was found by Miyaji[31] for a single crystal mat sample under pressures up to 22 kbar. It was confirmed that $\varepsilon_{(105)}$ for POM approximately satisfies the following hexagonal relationship:

$$\frac{\varepsilon_{(105)}}{d^2_{0,(105)}} = \frac{4}{3}\frac{\varepsilon_{(100)}}{a_0^2} + \frac{25}{c_0^2}\varepsilon_{(009)} \qquad (30)$$

The values of ε_l observed at 4903 bar are -0.0018, -0.0016 and ~ 0 for it-PP, it-P1B(I) and POM, respectively, which result in Poisson's ratios of 0.45, 0.47 and 0.5 according to equation (29). These values of the Poisson ratio are close to the typical value of 0.5 for the rubber-like materials.

Since no indications of splitting or broadening for the 300 reflection in P1B or the 100 reflection of POM were observed both the trigonal and the hexagonal phases of it-P1B and POM were preserved under the high pressures: the strain in the transverse direction must therefore be isotropic. The monoclinic it-PP crystal is more compressible along the *b*-axis than along the *a*-axis. Similar results for it-PP were recently obtained by Nakafuku[53].

This anisotropy of the transverse κ_0 found in it-PP was recently attributed by Tashiro, Kobayashi and Tadokoro[80] to crystalline dispersion due to rotation of the CH_3 groups. These authors drew this conclusion by comparing their theoretical calculations with the experimental κ_0s of Ito and coworkers. It is worth while noting that the magnitude of the transverse strains obtained for it-PP and it-P1B are similar to those for *o*-PE. The transverse strains found for POM, however, are about two-thirds of those for *o*-PE.

Poly(ethylene p*-oxybenzoate) α form*

According to Kusanagi *et al.*[81], the chain molecule of PEOB in the α crystal form assumes a large zigzag structure, consisting of:

(1) a small zigzag link of one monomeric unit

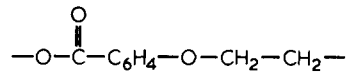

(2) an apex angle of 105° between the two axes of the adjacent monomeric zigzags; and

(3) a long arm of 6.0 Å, seven times as large as that for the fully-extended zigzag *o*-PE chain (0.85 Å). The observed[11,82] and calculated[83] values of E_l for PEOB(α) crystal are 5.9×10^4 and 2.4×10^4 bar, respectively, both of which are smaller by about one order of magnitude than the E_ls found for a polymer crystal made up from helical chains[10,11]. By uniaxial stretching, the longitudinal strain reaches about 5% at 2 kbar, as shown[82] in *Figure 17*.

Strains observed under high hydrostatic pressure are given[56] in *Figure 17*. Transverse strains are again similar to those for *o*-PE, while the strains along the fibre-axis are negligibly small ($-\varepsilon_{(006)} = 0.0012$ at 4903 bar), making a striking contrast with uniaxial stretching. Results for uniaxial stretching and hydrostatic compression indicate a Poisson ratio of $\nu = 0.49$, which strongly implies that the experimental Poisson ratio of the polymer crystal deduced by equation (29) is close to 0.5, irrespective of whether it is composed of helical or zigzag chains.

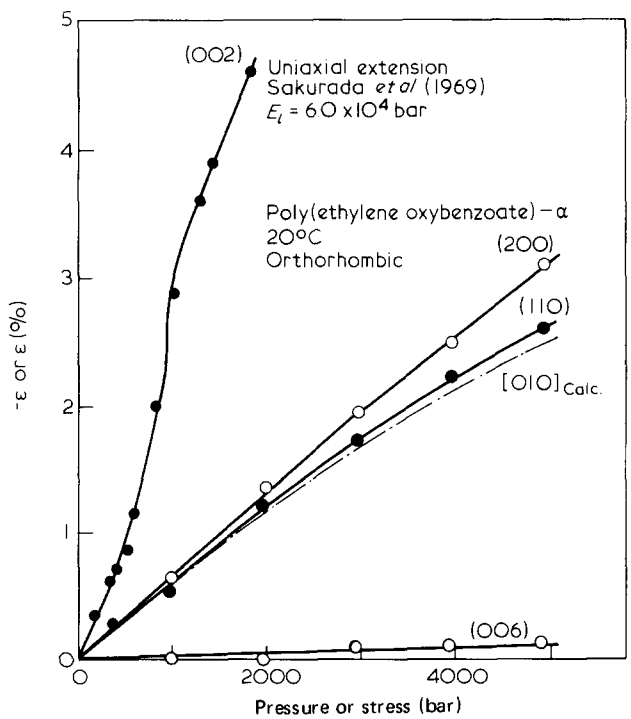

Figure 17 Pressure–strain curves for PEOB (α) compared with the uniaxial tension–strain curve in the fibre-axis direction obtained by Sakurada *et al.*[82]

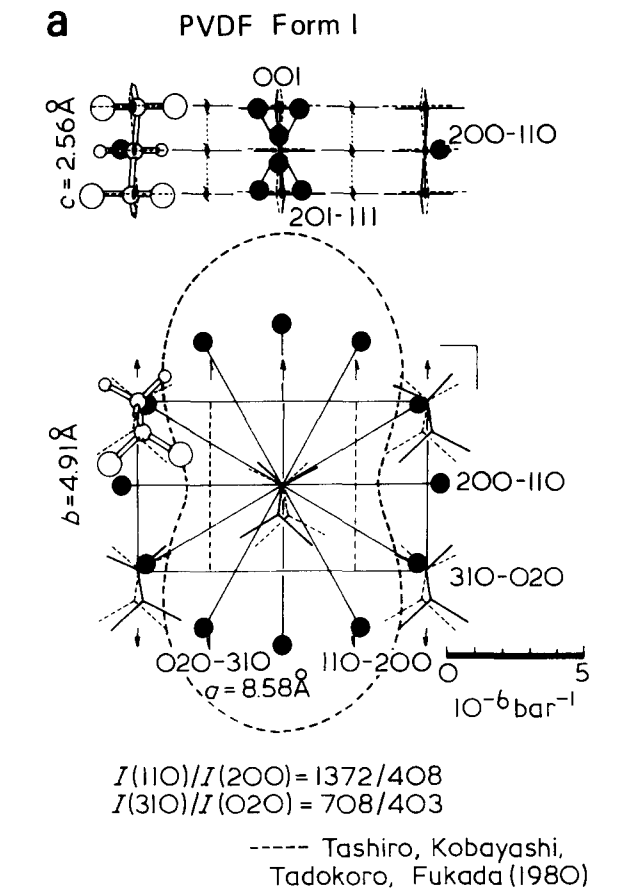

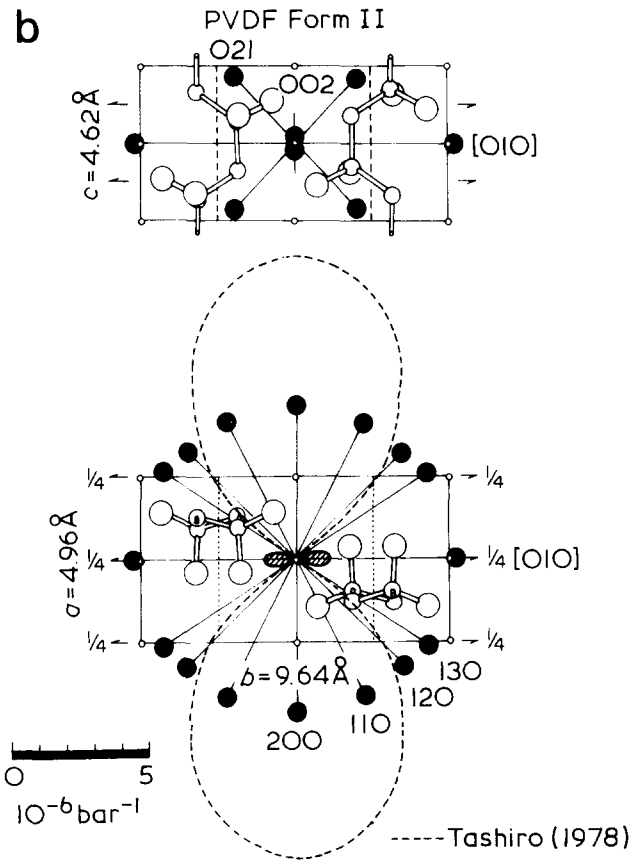

Figure 18 Observed and calculated anisotropy of κ_0 for (a) PVDF(I) and (b) PVDF(II). ●, Observed by Ito, Fujita and Okazaki[60]; – – –, calculated by Tashiro, Kobayashi, Tadokoro and Fukada[86] (a) and by Tashiro[85] (b)

Poly(vinylidene fluoride) forms I and II

PVDF crystallizes into several crystalline forms, of which form I and form II are most common, the former giving an orthorhombic and the latter a pseudo-orthorhombic (monoclinic, $\beta = 90°$) crystal structure[84]. The chain conformation is almost fully-extended planar zigzag in form I[84], in contrast to the contracted conformation of $tgt\bar{g}$ found in form II[84]. The results of the initial linear compressibility for the two forms are shown in *Figures 18a* and *18b*[60], where theoretical calculations by Tashiro *et al.*[85,86] are added for comparison. As shown, the experimental anisotropy in κ_0 is weak in the transverse direction for both forms. In form I, an attempt to obtain a rolled and doubly-oriented specimen was unsuccessful, but the two reflections on the equator, each made up of reflections from two lattice planes, showed almost the same pressure–strain relationship (see *Table 5*): there was no change in the breadth of the reflections with increasing pressure.

In *Figure 18a* plots of κ_0 were drawn, assuming that each of the two reflections on the equator represented the strain of a contributing lattice plane. For form I, theoretical results are about 30–50% larger than the experimental. For form II, experiments do not agree with theory, the latter predicting almost minimal compressibility along the *b*-axis. The experimental plot for the compressibility along this axis in form II (*Figure 18b*) was obtained by calculations using $\kappa_{0,(200)}$ and $\kappa_{0,(130)}$ in the following orthorhombic relationship:

$$\frac{9}{b_0^2}\kappa_{0,[010]} = \frac{1}{d_{0,(130)}^2}\kappa_{0,(130)} - \frac{1}{a_0^2}\kappa_{0,(200)} \qquad (31)$$

It was confirmed, for form II, that all the reflections (including the 021 on the first layer line) satisfy within the experimental error the orthorhombic relationship under high pressure. Moreover, the 040·210 reflection on the equator, which was fairly sharp, did not separate to the component reflections as pressure increased, giving $-\varepsilon_{(040\cdot210)} = 5.47 \times 10^{-6}P - 0.33 \times 10^{-9}P^2$ ($P \leqslant 5880$ bar) in agreement with the calculated strain in the [010] direction (see *Table 5*).

Along the fibre-axis, $\kappa_{0,(002)}$ for form II was found smaller than $\kappa_{0,(001)}$ in form I. This is difficult to explain from equation (29) if approximately the same values for the Poisson ratio are assumed for the two forms, because E_l values for forms I and II reported by Sakurada and Kaji[11] equal 177×10^4 and 59×10^4 bar, respectively as expected for the chain conformations involved.

EFFECT OF HYDROGEN BONDING

Nylon-6[87] and at-PVA[88,89] crystals are made up of the so-called sheet structures in which intermolecular two-dimensional hydrogen bonding develops to form the molecular 'sheets'. These sheets are stacked by weak van der Waals forces. These polymer crystals are expected to exhibit anisotropy in mechanical properties, characteristic of the sheet structure. Sakurada and Kaji demonstrated[16] that the Young's moduli in directions perpendicular to the fibre-axis for nylon-6 and at-PVA crystals are highly anisotropic depending on the direction of the stress in the hydrogen-bonded molecular sheet.

The results of the ε–P relationships for Ny-6(α) and Ny-6(γ) crystals obtained by Ito, Hirata and Fujita[58] are shown in *Figure 19*. For Ny-6(α) and Ny-6(γ) crystals, a

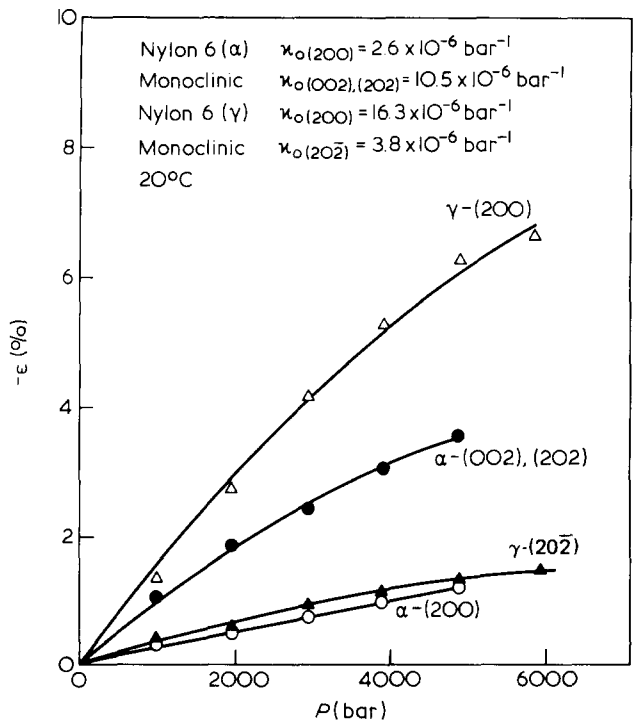

Figure 19 Pressure–strain curves for Ny-6(α) and Ny-6(γ)[58]

clear-cut relationship was found among the linear strain, initial linear compressibility and sheet structure. To show this, the normals of the observed planes, the directions of the sheets and the observed κ_0s are shown in *Figures 20a* and *20b* on structure diagrams projected on the *ac*-plane of the monoclinic crystals of Ny-6(α) and Ny-6(γ)[90] (where the hydrogen bonds were indicated with dotted lines). For the γ-form, κ_0 is 4.3 times larger in the direction perpendicular to the sheet than parallel to it. Because of this strong anisotropy, the 001·200 doublet reflection became well separated with increasing pressure[58]. Similar results were obtained for the α-form. Thus the inversion of the sheet direction involved in the α→γ transition[90] of Ny-6 is distinctly reflected in the anisotropy of the linear compressive strains induced by the hydrostatic pressure. This is consistent with the uniaxial stretching results of Sakurada and Kaji[16], who demonstrated that the transverse Young's modulus in the direction of the sheet ($E_t = 11.4 \times 10^4$ bar) for Ny-6 crystals (α- and γ-forms) is 2.7 times larger than that perpendicular to the sheet ($E_t = 4.3 \times 10^4$ bar).

Here it is interesting to compare the experimental results of Ito *et al.* for transverse κ_0 with theroetically calculated values obtained by Tashiro and Tadokoro[91] and Tadokoro *et al.*[92] (*Figures 20a* and *20b*). For the γ-structure (*Figure 20b*), the agreement between the experimental and theoretical results is adequate. However, the number of experimental points is too small to draw the whole dumbbell shape. This shape, which is variable depending upon the degree of the anisotropy, is theoretically required if the monoclinic relationship across a lateral cross-section of the lattice holds during deformation.

For the α-structure (*Figure 20a*), the theoretical result could well represent the experimental anisotropy, but its numerical value fails to explain the experimental data. This is ascribed by Tashiro and Tadokoro[91] to the unusually small distances for some of the intermolecular hydrogen bonds found in the α-structure reported by Holmes *et al.*[87], on which their theoretical calculations were based.

Based on these successful results for Ny-6(α) and Ny-6(γ) crystals, we can now plot κ_0 for at-PVA measured along the normals of the observed planes (*Figure 21*). Here the anisotropy of the linear compressibility, though not so striking as in Ny-6 crystals, is found to be consistent with the sheet structure given by Sakurada[16] and Okada[93] in which the molecular sheet is parallel to the *ab*-plane. Sakurada and Kaji found the same anisotropy[16] in Young's modulus. However, the recent theoretical calculations for the κ_0 in PVA by Tashiro, Kobayashi and Tadokoro[26] revealed that this anisotropy may be explained using Bunn's model[88,16] where the sheet is parallel to the *ab*-plane.

Calculated results based on Bunn's model obtained by Tashiro *et al.* (who did not extend their calculations to the

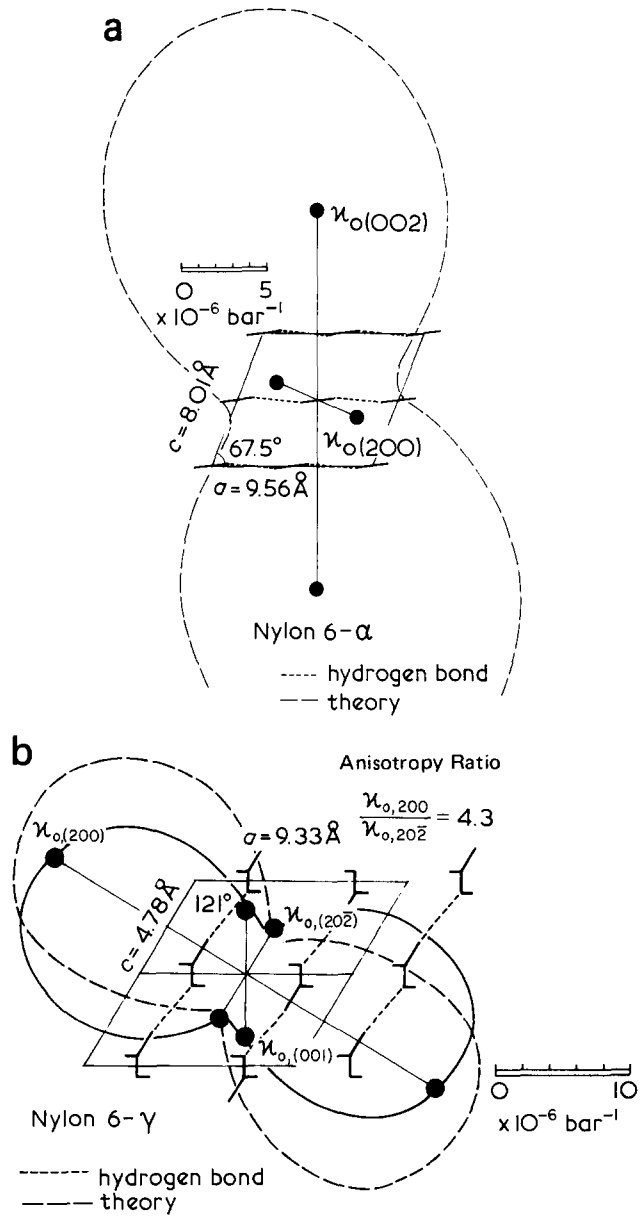

Figure 20 Observed and calculated anisotropy of κ_0 in the *ac* plane of (a) Ny-6(α) and (b) Ny-6(γ). ●, Observed by Ito, Hirata and Fujita[58]; – – –, calculated by Tashiro and Tadokoro[91] and Tadokoro *et al.*[92]

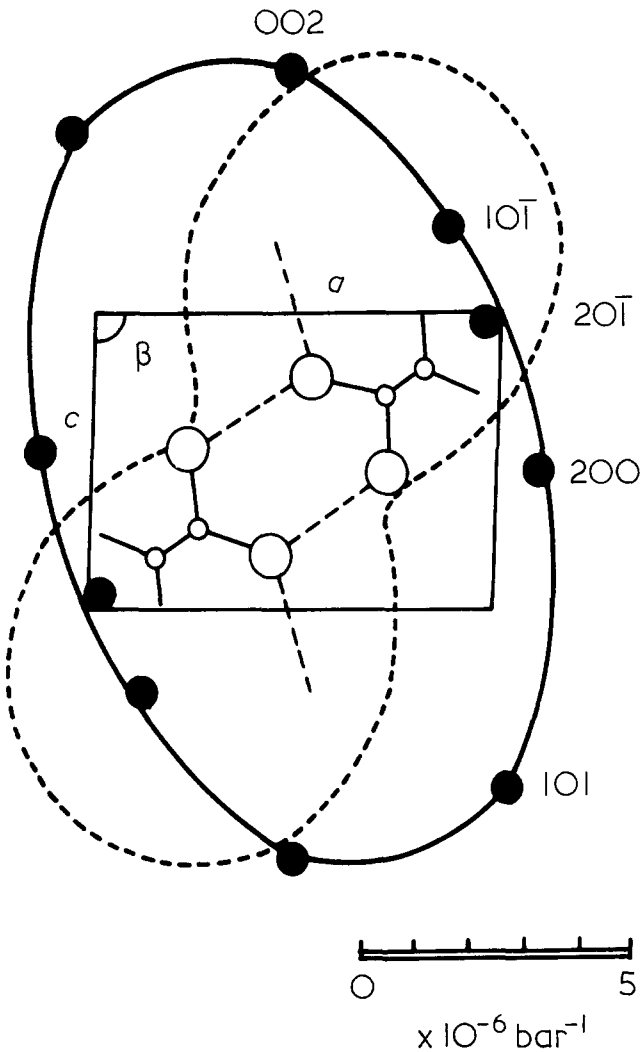

Figure 21 Calculated and observed anisotropy of κ_0 in the *ac* plane of at-PVA. – – –, Calculated by Tashiro, Kobayashi and Tadokoro[26]; ●, observed by Ito, Hirata and Fujita[58]

model by Sakurada and Okada) are shown by the broken line in *Figure 21*, where there is seen, in spite of a discrepancy amounting to 40° between the long axes, an essential agreement between the calculated and the observed (full line) linear compressibilities. The direction of the hydrogen bonds within the PVA crystal structure for both models deviate markedly from the plane of the sheet. This may reduce the direct correlation between the anisotropy of the linear compressibility and the direction of the sheet, especially if hydrogen bonding contributes to an appreciable degree to the deformation of the crystal under the hydrostatic compression.

CONCLUSIONS

Table 5 lists data for various polymer crystals: the crystal density ρ_{cryst}, the packing density, the observed lattice planes, the coefficients of the polynomial giving the linear compressive strain at 20°C and the initial linear and bulk compressibilities. β_0 values were deduced by calculation from κ_0 values, assuming conservation of the angle between the principal axes of the zero pressure unit cell.

Of the compressibilities obtained to date, it-P4M1P gives the largest value ($\beta_0 = 36.7 \times 10^{-6}$ bar^{-1}) and carbon fibre the smallest ($\beta_0 = 3.0 \times 10^{-6}$ bar^{-1})[61], as seen from *Table 5*. Since the graphite crystal has a two-dimensional covalent skeleton, β_0 for carbon fibre takes an unusually small value and should be excepted from the typical values of the polymer crystal which results from one-dimensional covalent chains. Values for graphite have been reported by Drickamer *et al.*[95] ($\beta_0 = 2.86 \times 10^{-6}$ bar^{-1}) and Ito and Nakamura[61] ($\beta_0 = 3.3 \times 10^{-6}$ bar^{-1}).

With this exception then, the compressibilities of the polymer crystals were found to lie in a relatively narrow range from 36.7×10^{-6} bar^{-1} for it-P4M1P to 11.7×10^{-6} bar^{-1} for POM, at-PVA, PEO(I)[55], PVDF(I) and PVDF(II). This is illustrated by the horizontal hatched zone in *Figure 22* where β_0 for elemental solids have been plotted against the atomic number for comparison[96].

In this Figure, the top hatched zone (representing polymer crystals) just covers the compressibilities of the alkali metals. Indeed, bulk compressibilities of the polymer crystals correspond to those of the alkali metals. However, the linear compressibility of the polymer crystal is strongly anisotropic among the fibre and lateral axes: along the fibre axis the compressibility is of the order of 10^{-7} bar^{-1}, only twice as large as the linear compressibility of diamond[95], $\kappa_0 = 0.060 \times 10^{-6}$ bar^{-1} (the lowest value for a solid material).

The compressibility of the polymer crystal decreases with increasing density (*Figure 23a*) where β_0 was plotted against density. The result is reasonable since the bulk density roughly reflects the number of atoms and covalent bonds per unit volume of those organic molecular crystals. It is worth noting that β_0 for adamantane lies on the β_0–ρ_{cryst} curve derived for polymer crystals. Adamantane has a face-centred cubic structure, each lattice point representing a cage-like molecule of adamantane[97]. The whole structure is thus held together by weak van der Waals attractions acting between the saturated hydrocarbon molecules. However, when derived from the crystal density, β_0 for adamantane takes a value predicted for a polymer crystal which loses one degree of freedom of compressibility along the fibre axis because of the incompressibility of its covalent skeleton.

The adamantane crystal displays a cubic→tetragonal crystal–crystal transition at $P = 4.71$ kbar at room temperature ($T = 293$K)[98], when the crystal contracts 3.6% along the *c*-axis of the tetragonal structure and

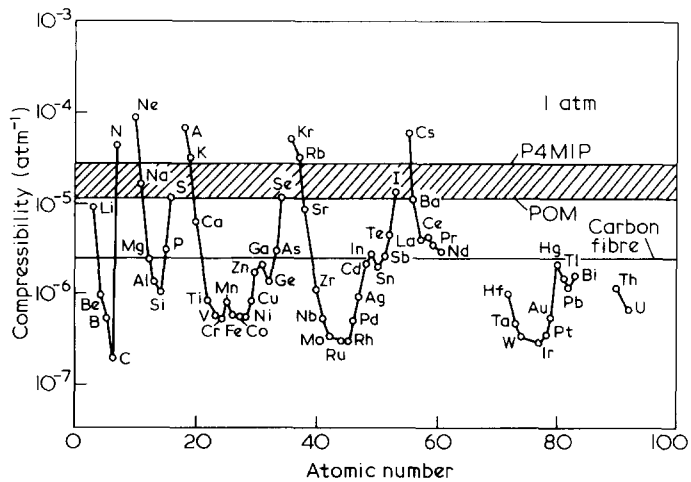

Figure 22 Range of magnitude of β_0 for the polymer crystals superposed on the β_0–atomic number diagram for the solid elements taken from Hamann[96]

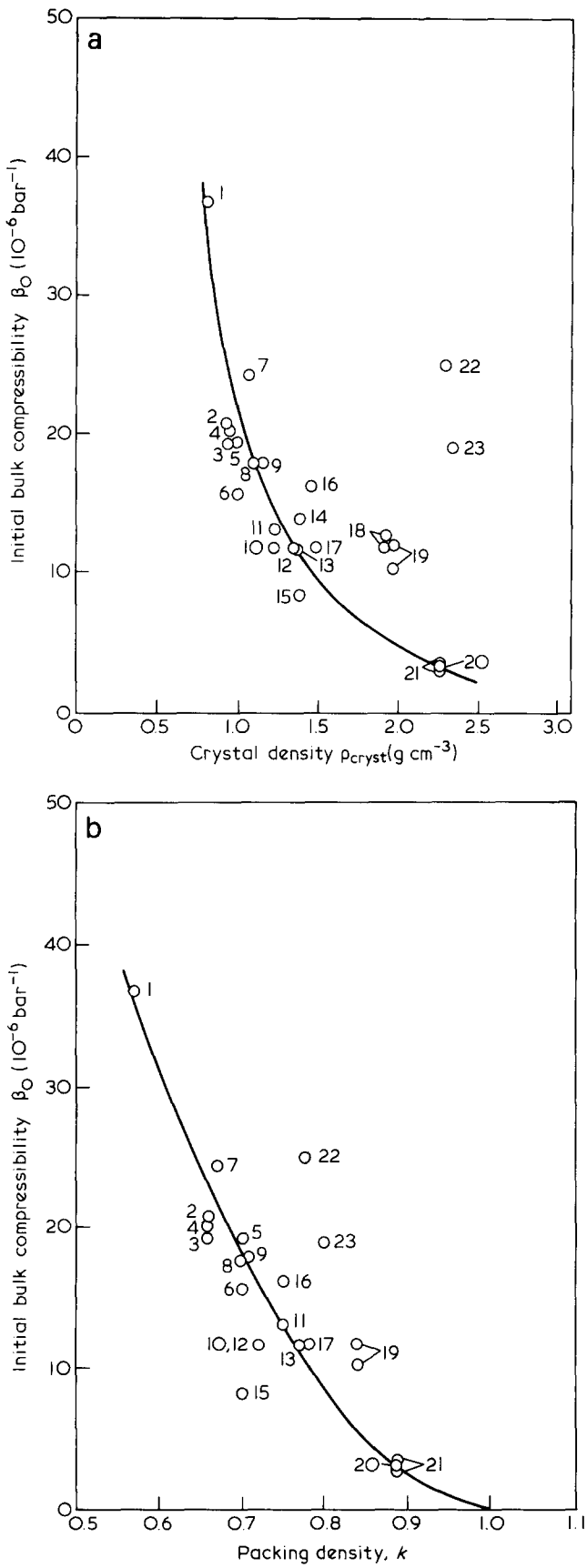

Figure 23 β_0 vs. density of the crystal plots (a) and β_0 vs. packing density plots (b) for various polymer crystals and some low-molecular weight organic crystals. 1, it-P4M1P; 2, it-PP; 3, n-heptacosane; 4, it-P1B(I); 5, LDPE; 6, *o*-PE; 7, adamantane; 8, PTMO(I); 9, Ny-6(γ); 10, PEO(I); 11, Ny-6(α); 12, hexamethylenetetramine; 13, at-PVA; 14, PEOB(α); 15, pentaerythritol; 16, poly(ethylene terephthalate); 17, POM; 18, PVDF(II); 19, PVDF(I); 20, carbon fibre; 21, graphite; 22, PTFE(IV); 23, PTFE(II). For the abbreviations for the various polymers, see text

elongates[49] 1.1% in the lateral direction—a net effect of volume contraction of 1.4% (*Figure 24*). Such linear elongation and contraction during a pressure-induced crystal–crystal transition was also found for the II→III transition of PTFE crystal.

β_0s for PTFE in the II and IV crystal modifications are extraordinarily large and deviate from the expected relationship. To eliminate the effect of the heavy fluorine atoms (*Figure 23b*), β_0 was plotted against packing density k instead of the bulk density. β_0 decreases with increasing k in a manner similar to that in *Figure 23a*. The following empirical rule was found between β_0 and k:

$$\beta_0(10^{-6}\,\text{bar}^{-1}) = 7.65(1-k) + 177(1-k)^2 \qquad (32)$$

A slight reduction in the deviation of the plots was obtained in *Figure 23b* compared with *Figure 23a*. Even using β_0 vs. k plots, the PTFE crystal is extraordinarily compressible, though the plots shift in the right direction towards the normal behaviour for a polymer crystal.

These extraordinarily large compressibilities are only one of the peculiar properties exhibited by PTFE crystal, which include the solid state transition at room temperature which occurs by the twisting or untwisting and rotation of the rod-like helical chain molecules[67].

Finally, it is interesting to note that, in spite of having fewer covalent bonds, organic low molecular weight crystals give β_0s that are indistinguishable from, or even smaller than β_0s for polymer crystals in both the β_0 vs. ρ_{cryst} and β_0 vs. k plots. For this, a large number of defects and distortions particularly insisted upon for the polymer crystals[99] may give the reason.

NOTE ADDED AFTER COMPLETION OF MANUSCRIPT

The author has been informed by Dr Nakafuku of Kochi University of studies on PVDF(I) and PVDF(II) by

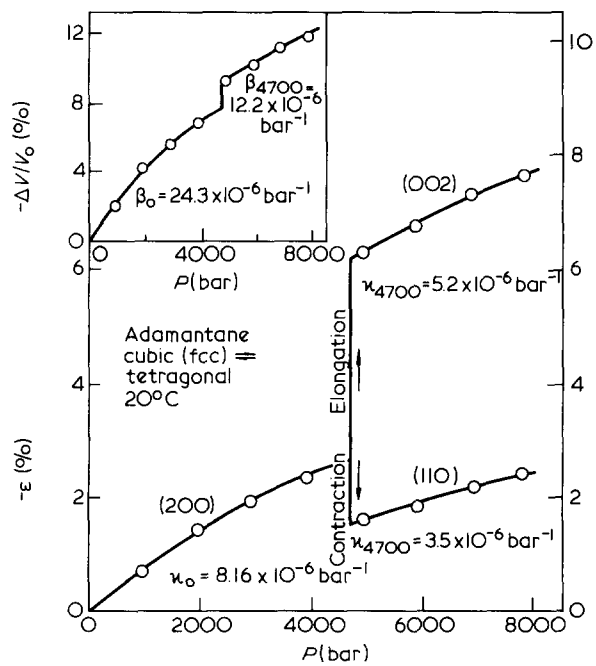

Figure 24 Pressure–strain and pressure–volumetric strain curves for adamantane at 293K. The fcc ⇄ tetragonal crystal–crystal transition occurs at P = 4.71 kbar

Newman, Yoon and Pae (NYP)[100] and by Nakafuku[101]. Data are listed in *Table 5*.

The present author's opinion is that:

(1) NYP used the Tait equation to analyse the data;

(2) for form I, there is a fairly good agreement between the results for κ_0 obtained by NYP and by Ito, Fujita and Okazaki (IFO)[60] although the former are 10–25% smaller than the latter;

(3) for form II, there is substantial disagreement. Along the *a*-axis, κ_0 (NYP) is about twice as large as κ_0 (IFO), while along the *b*-axis, κ_0 (NYP) was negligibly small. The κ_0 (IFO) value in this direction was 5.9×10^{-6} bar^{-1}. κ_0 for the (200), (120), (130) and (040)·(210) planes were not described in the NYP paper. These were obtained in the IFO study with reasonable accuracy (*Table 5*);

(4) β_0 for form I (NYP) ($\beta_0 = 8.5 \times 10^{-6}$ bar^{-1}) is about 30% smaller than that obtained by IFO ($\beta_0 = 11.8 \times 10^{-6}$ bar^{-1}). For form II, there is fortuitous agreement between the data for β_0 (NYP) and β_0 (IFO). The latter authors found β_0 for form I and form II with similar values. This is reasonable because ρ_{cryst} is about the same for both modifications (*Table 5*);

(5) There is essential agreement between the results obtained by Nakafuku and by IFO. Nakafuku also found almost linear isotropic compressibilities in the transverse direction for both form I and form II. His calculated value for $\kappa_{0,c}$ in the fibre axis direction for form II (0.76×10^{-6} bar^{-1}) is about three times larger than the value observed by IFO (0.27×10^{-6} bar^{-1}) while it amounts to half the value observed by NYP (1.3×10^{-6} bar^{-1});

(6) Nakafuku studied the temperature dependence of the linear compressibilities.

REFERENCES

1 Peterlin, A. *Polym. Eng. Sci.* 1979, **19**, 118
2 Kardos, J. L., Piccarolo, S. and Halpin, J. C. *Polym. Eng. Sci.* 1978, **18**, 505
3 Clements, J., Jakeways, R. and Ward, I. M. *Polymer* 1978, **19**, 639
4 McCullough, R. L., Wu, C. T., Seferis, J. C. and Lindenmeyer, P. H. *Polym. Eng. Sci.* 1976, **16**, 371
5 Takayanagi, M., Imada, K. and Kajiyama, T. *J. Polym. Sci. (C)* 1966, **15**, 263
6 Perkins, W. G. and Porter, R. S. *J. Mater. Sci.* 1977, **12**, 2355
7 Capaccio, G. and Ward, I. M. *Polymer* 1974, **15**, 233
8 'Ultra-high Modulus Polymers' (Eds. A. Ciferri and I. M. Ward), Applied Science Publishers, London, 1979
9 Sakurada, I., Nukushina, Y. and Ito, T. *J. Polym. Sci.* 1962, **57**, 651
10 Sakurada, I., Ito, T. and Nakamae, K. *J. Polym. Sci. (C)* 1966, **15**, 75
11 Sakurada, I. and Kaji, K. *J. Polym. Sci. (C)* 1970, **31**, 57
12 Dulmage, W. J. and Contois, L. E. *J. Polym. Sci.* 1958, **28**, 275
13 Reuss, A. *Z. Angew. Math. Mech.* 1929, **9**, 49
14 Geil, P. H. *Polymer Colloquium, Kyoto, 1977, Prepr.* 48; Hasegawa, H., Hagerling, C. W., Hoffman, R. W. and Geil, P. H. *Polym. Prepr. Jpn.* 1979, **28**, 1870
15 Ito, T. and Marui, H. *Polym. J.* 1971, **2**, 768
16 Sakurada, I. and Kaji, K. *Makromol. Chem. Suppl.* 1975, **1**, 599
17 Müller, A. *Proc. Roy. Soc., London (A)* 1936, **154**, 624; *Ibid.* 1941, **178**, 227
18 Brandt, W. *J. Chem. Phys.* 1957, **26**, 262
19 Odajima, A. and Maeda, T. *J. Polym. Sci. (C)* 1966, **15**, 55
20 Barker Jr., R. E. *J. Appl. Phys.* 1967, **38**, 4234
21 Pastine, D. J. *J. Chem. Phys.* 1968, **49**, 3012
22 Broadhurst, M. G. and Mopsik, F. I. *J. Chem. Phys.* 1970, **52**, 3634
23 Wobser, G. and Blasenbrey, S. *Kolloid Z. Z. Polym.* 1970, **241**, 985
24 Midha, Y. R. and Nanda, V. S. *Macromolecules* 1977, **10**, 1031
25 Tashiro, K., Kobayashi, M. and Tadokoro, H. *Macromolecules* 1978, **11**, 908
26 Tashiro, K., Kobayashi, M. and Tadokoro, H. *Macromolecules* 1978, **11**, 914
27 Kobayashi, M. *J. Chem. Phys.* 1979, **70**, 509
28 Goel, S. C., Nanda, V. S. and Jain, R. K. *Macromolecules* 1979, **12**, 339
29 Kobayashi, M. and Tadokoro, H. *J. Chem. Phys.* 1977, **66**, 1258
30 Bhateja, S. K. and Pae, K. D. *J. Macromol. Sci. (Rev. Macromol. Chem.)* 1975, **C13**, 77
31 Miyaji, H. *J. Phys. Soc. Jpn.* 1975, **39**, 1346
32 Slater, J. C. 'Introduction to Chemical Physics', McGraw-Hill, New York, 1939
33 Wu, C. K., Jura, G. and Shen, M. *J. Appl. Phys.* 1972, **43**, 4348
34 Kitagawa, T. and Miyazawa, T. *Adv. Polym. Sci.* 1972, **9**, 335
35 Yamamoto, T., Miyaji, H. and Asai, K. *Jpn. J. Appl. Phys.* 1977, **16**, 1891
36 Piermarini, G. J. and Weir, C. E. *J. Res. Natl. Bur. Stand. (A)* 1962, **66**, 325
37 Sham, T. P., Newman, B. A. and Pae, K. D. *J. Mater. Sci.* 1977, **12**, 771
38 Hikosaka, M., Minomura, S. and Seto, T. *26th IUPAC Congress 1977*, Abstracts p. 1385; Hikosaka, M., Seto, T. and Minomura, S. *Polym. Prepr. Jpn.* 1977, **26**, 421
39 Kabalkina, S. S. and Vereshchagin, L. F. *Dokl. Akad. Nauk. SSSR* 1962, **143**, 818
40 Ito, T. *Rev. Sci. Instrum.* 1974, **45**, 1560
41 Ito, T. 'High Pressure Science and Technology', Vol. 1 (Eds. K. D. Timmerhaus and M. S. Barber), Plenum, New York, 1979, p. 482
42 Nakafuku, C. and Takemura, T. *Jpn. J. Appl. Phys.* 1975, **14**, 599
43 Yasuniwa, M., Enoshita, R. and Takemura, T. *Jpn. J. Appl. Phys.* 1976, **15**, 1421
44 Nakafuku, C. *Polymer* 1978, **19**, 149
45 Ito, T. and Nakamura, R. *21st Annual Meeting of the Society of Polymer Science, Japan, Tokyo, 1972, Prepr.* p. 172
46 Ito, T. and Nakamura, R. *23rd Discussion Meeting of the Society of Polymer Science, Japan, Tokyo, 1974, Prepr.* p. 859
47 Hatakeyama, T., Hashimoto, T. and Kanetsuna, H. *Colloid Polym. Sci.* 1974, **252**, 15
48 Ito, T. *Kobunshi (High Polym. Jpn.)* 1972, **21**, 82
49 Ito, T. *Nippon Kesshyo Gakkaishi (J. Crystallogr. Soc. Jpn.)* 1974, **16**, 318
50 Ito, T. *Sen'i Gakkaishi (J. Soc. Fiber Sci. Technol. Jpn.)* 1976, **32**, P–46
51 Ito, T. *Kobunshi (High Polym. Jpn.)* 1976, **25**, 750
52 Ito, T., Ito, S., Ozawa, N. and Nakagawa, Y. *24th Annual Meeting of the Society of Polymer Science, Japan, Tokyo, Prepr.* p. 482, 1975
53 Nakafuku, C. *Polym. Prepr. Jpn.* 1979, **28**, 440
54 Ito, T., Tanabe, S. and Yamane, S. *22nd Annual Meeting of the Society of Polymer Science, Japan, Kyoto, Prepr.* p. 15, 1973
55 Ito, T., Hirata, T. *Polym. Prepr. Jpn.* 1977, **26**, 420
56 Ito, T. *Polym. Prepr. Jpn.* 1976, **25**, 498
57 Ito, T., Hirata, T. and Fujita, S. *Polym. Prepr. Jpn.* 1978, **27**, 530
58 Ito, T., Hirata, T. and Fujita, S. *J. Polym. Sci. (Polym. Phys. Edn.)* 1979, **17**, 1237
59 Ito, T. and Fujita, S. *Polym. Prepr. Jpn.* 1978, **27**, 531
60 Ito, T., Fujita, S. and Okazaki, S. *Polym. Prepr. Jpn.* 1980, **29**, 479
61 Ito, T. and Nakamura, R. *21st Annual Meeting of the Society of Polymer Science, Japan, Tokyo, 1972, Prepr.* p. 173
62 Baskin, Y. and Meyer, L. *Phys. Rev.* 1955, **100**, 544
63 Bunn, C. W. *Trans. Faraday Soc.* 1939, **35**, 482
64 Swan, P. R. *J. Polym. Sci.* 1962, **56**, 403, 409
65 Born, M. and Huang, T. 'Dynamical Theory of Crystal Lattices', Clarendon, Oxford, 1956
66 Bunn, C. W. and Howells, E. R. *Nature* 1954, **174**, 549
67 Clark, E. S. and Muus, L. T. *Z. Krist.* 1962, **117**, 119
68 Matsushige, K., Enoshita, R., Ide, T., Yamauchi, N., Taki, S. and Takemura, T. *Jpn. J. Appl. Phys.* 1977, **16**, 681
69 Kusanagi, H., Chatani, Y., Takase, M. and Tadokoro, H. *J. Polym. Sci. (Polym. Phys. Edn.)* 1978, **16**, 131
70 Griffith, J. H. and Rånby, B. G. *J. Polym. Sci.* 1960, **44**, 369
71 Bassi, I. W., Bonsignori, O., Lorenzi, G. P., Pino, P., Corradini, P. and Temussi, P. A. *J. Polym. Sci. (A-2)* 1971, **9**, 193
72 Kitaigorodskii, A. I. 'Organic Chemical Crystallography', Consultants Bureau, New York, 1961, p. 106
73 Wunderlich, B. 'Macromolecular Physics', Vol. 1, Academic Press, New York, 1973, p. 106
74 Hearmon, R. F. S. 'An Introduction to Applied Anisotropic Elasticity', Oxford University, London, 1961
75 Natta, G. and Corradini, P. *Nuovo Cimento, Suppl.* 1960, **15**, 40
76 Natta, G., Corradini, P. and Bassi, I. W. *Nuovo Cimento, Suppl.* 1960, **15**, 52

77 Uchida, T. and Tadokoro, H. *J. Polym. Sci. (A-2)* 1967, **5**, 63
78 Tadokoro, H. 'Structure of Crystalline Polymers', Wiley, New York, 1979
79 Shimanouchi, T., Asahina, M. and Enomoto, S. *J. Polym. Sci.* 1962, **59**, 93; Asahina, M. and Enomoto, S. *J. Polym. Sci.* 1962, **59**, 101
80 Tashiro, K., Kobayashi, M. and Tadokoro, H. *Symposium on Molecular Structure, Tokyo, Japan* 1979, p. 110
81 Kusanagi, H., Tadokoro, H., Chatani, Y. and Suehiro, K. *Macromolecules* 1977, **10**, 405
82 Sakurada, I., Nakamae, K., Kaji, K. and Wadano, S. *Kobunshi Kagaku (Chem. High Polym. Jpn.)* 1969, **26**, 561
83 Tashiro, K., Kobayashi, M. and Tadokoro, H. *Macromolecules* 1977, **10**, 413
84 Hasegawa, R., Takahashi, Y., Chatani, Y. and Tadokoro, H. *Polym. J.* 1972, **3**, 600
85 Tashiro, K. *Thesis*, Faculty of Science, Osaka University (1978)
86 Tashiro, K., Kobayashi, M., Tadokoro, H. and Fukada, E. *Macromolecules* 1980, **13**, 691
87 Holmes, D. R., Bunn, C. W. and Smith, D. J. *J. Polym. Sci.* 1955, **42**, 159
88 Bunn, C. W. *Nature* 1948, **161**, 929
89 Nitta, I., Taguchi, I. and Chatani, Y. *Sen'i Kenkyusho Nenpo (Ann. Rep. Inst. Fiber Res. Osaka Univ.)* 1957, **10**, 1
90 Arimoto, H., Ishibashi, M., Hirai, M. and Chatani, Y. *J. Polym. Sci. (A)* 1965, **3**, 317
91 Tashiro, K. and Tadokoro, H. *Polym. Prepr. Jpn.* 1978, **27**, 1668
92 Tadokoro, H., Tashiro, K., Kobayashi, M. and Chatani, Y. *Polym. Prepr.* 1979, **20**, 240
93 Okada, N. *Thesis*, Faculty of Engineering, Kyoto University (1957)
94 Ito, T. and Hirata, T. unpublished data
95 Drickamer, H. G., Lynch, R. W., Clendenen, R. L. and Perez-Albuerne, E. A. 'Solid State Physics', Vol. 19, (Eds. F. Seitz and D. Turnbull), Academic Press, New York, 1966, p. 135
96 Hamann, S. D. 'Physico-Chemical Effects of Pressure', Butterworths, London, 1957
97 Nowacki, W. *Helv. Chim. Acta* 1945, **28**, 1233
98 Ito, T. *Acta Crystallogr. (B)* 1973, **29**, 364
99 Hosemann, R. *Polymer* 1962, **3**, 349; *Ibid.* 1963, **4**, 199
100 Newman, B. A., Yoon, C. H. and Pae, K. D. *J. Mater. Sci.* 1979, **14**, 2391
101 Nakafuku, C. *Rep. Prog. Polym. Phys. Jpn.* 1980, **23**, 187
102 Pahiya, O. P. and Nanda, V. S. *Polym. J.* 1982, **14**, 245